World Electric Vehicle Journal

MDPI

Article

Investigation of Drive Performance of Motors in Electric Loaders with Unequal Transmission Ratios—A Case Study

Xiaotao Fei [1,2], Shaw Voon Wong [2,*], Muhammad Amin Azman [2], Peng Liu [1,3] and Yunwu Han [1,*]

1 Department of Automobile Engineering, Jiangsu Vocational College of Electronics and Information, Huai'an 223003, China; gs59709@student.upm.edu.my (X.F.)
2 Department of Mechanical & Manufacturing, Faculty of Engineering, Universiti Putra Malaysia, Selangor 43400, Malaysia
3 Department of Mechanical and Manufacturing Engineering, Faculty of Engineering & Built Environment, Universiti Kebangsaan Malaysia, UKM Bangi, Selangor Darul Ehsan 43600, Malaysia
* Correspondence: wongsv@upm.edu.my (S.V.W.); hanyw08@jsei.edu.cn (Y.H.)

Abstract: Research on electric wheel loaders (EWLs) has predominantly focused on battery management, hybrid technologies, and energy recovery. However, the influence of motor types and drivetrains on the drive performance of EWLs has received little attention in previous studies. This case study addresses this gap by examining different EWL configurations and analyzing the drive theory and force requirements by integrating classic vehicle theory with EWL-specific characteristics. The study compares an original EWL, equipped with Permanent Magnet Synchronous Motors (PMSMs) on both the front and rear axles with identical transmission ratios of 22.85, to a modified EWL, which features a Switched Reluctance Motor (SRM) on the front axle and a transmission ratio of 44.05. Walking and shoveling tests were conducted to evaluate performance. The walking test results reveal that, at motor speeds of 200 rpm, 400 rpm, and 600 rpm, energy consumption in R-drive mode is 68.56%, 71.88%, and 74.87% of that in F-drive mode when two PMSMs are used. When an SRM is applied with a transmission ratio of 44.05, these values shift to 73.90%, 70.35%, and 67.72%, respectively. This demonstrates that using the rear motor alone for driving under walking conditions can yield greater energy savings. The shoveling test results indicate that distributing torque according to wheel load reduces rear wheel slippage, and the SRM with a transmission ratio of 44.05 delivers sufficient drive force while operating within a high-efficiency speed range for the EWL.

Keywords: motor; drive performance; electric wheel loader; transmission ratio; torque distribution

check for updates

Citation: Fei, X.; Wong, S.V.; Azman, M.A.; Liu, P.; Han, Y. Investigation of Drive Performance of Motors in Electric Loaders with Unequal Transmission Ratios—A Case Study. *World Electr. Veh. J.* **2024**, *15*, 459. https://doi.org/10.3390/wevj15100459

Academic Editor: Michael Fowler

Received: 21 August 2024
Revised: 28 September 2024
Accepted: 9 October 2024
Published: 10 October 2024

1. Introduction

A wheel loader (WL) is a kind of earth-moving machinery that is widely applied in constructions, mines and ports all around the world. As the electrification of heavy vehicles [1,2] and construction machineries [3–5] has become a research trend, efforts are also being made to electrify WLs. A WL usually works in four stages, including loading material, carrying material, dumping material and returning to the start point, in a typical working cycle [6]. Therefore, the drive motor is utilized in at least two stages of a working cycle. During the initial stage of loading material, the WL moves at a very slow or near-zero speed. Similarly, during the dumping stage, the WL body is almost stationary. If a WL is powered by a diesel engine, the engine must operate at a high-idle speed to support the hydraulic system. In contrast, in an electric wheel loader (EWL), the drive motor can remain stationary during these stages. This significantly reduces energy consumption when electric motors are used in the drivetrain of a WL, regardless of whether it is a pure electric drive, hybrid drive, or fuel cell electric drive. In the field of energy-saving research on EWLs, battery management [7–9], hybrid technologies [10–12], and energy recovery [13,14] are mostly focused on.

In most electric passenger vehicles, motors are essential for propelling the drive system, and optimizing their performance has been a key focus. Yang et al. [15] proposed a variable voltage control strategy to reduce losses in Permanent Magnet Synchronous Motor (PMSM) systems. This strategy improved inverter efficiency by 12.8% and motor efficiency by 0.77%. However, the approach has not yet been validated through real-world tests. Minh D et al. [16] designed and evaluated a Brushless Direct Current (BLDC) motor with different rotor configurations and Halbach array magnets. Their design demonstrated enhanced torque and efficiency. Dorrell et al. [17] examined different motor designs for hybrid electric vehicles (HEVs), while Wu et al. [18] introduced two new dual-motor powertrains that enhance electric vehicle (EV) efficiency through optimized gear ratios and mode shifting. These studies on EVs provide valuable references for research into motor applications in EWLs.

Each type of power motor exhibits distinct performance characteristics, and the choice of motor has a significant impact on the operational efficiency of EWLs. Several studies have explored different motor applications in EWLs. Jin et al. [19] developed and tested a power-distributed WL, incorporating two PMSMs for the driving and braking systems, and an induction motor (IM) for the hydraulic system. Li et al. [20] designed a fuel cell hybrid WL featuring two AC synchronous motors, each assigned to the driving and hydraulic systems, respectively. Additionally, Liu et al. [21] investigated the use of Switched Reluctance Motors (SRMs) in WLs, demonstrating that SRMs can enhance both performance and reliability. These studies highlight that PMSMs, IMs, and SRMs are viable motor options for EWLs. Further, M. Yildirim et al. [22], through a comparative analysis of four different motor types, concluded that SRMs are the most suitable motors for electric vehicles.

Despite these advances, previous research has not quantitatively assessed the influence of motor type on the overall performance of WLs. To address this, Li et al. [23] conducted a series of tests to evaluate the performance of three different motor types applied in EWLs. Their findings indicated that pure EWLs exhibit optimal performance when the walking system is powered by an SRM and the hydraulic system is driven by a PMSM. Xu et al. [24] further developed an SRM for an EWL with four in-wheel drive using simulation and test bench methods. However, none of these studies conducted real-world testing on a full-scale EWL.

In light of this gap, the present research proposes a novel drivetrain structure for an EWL, applying a PMSM to the rear axle and an SRM to the front axle. This study makes two key contributions. First, it introduces a new drivetrain configuration for EWLs, demonstrating that both configurations achieve energy savings when power is supplied by the rear motor compared to when the front motor provides power. Second, it empirically verifies the performance of the electric drive walking system using two different setups—one with dual PMSMs driving both axles, and another with an SRM on the front axle and a PMSM on the rear axle in the modified drivetrain. The main content is organized as follows. Section 2 provides a brief overview of the development and features of pure EWLs; Section 3 outlines the research methodology, including EWL drive theory, drive force requirement analysis, front axle structural modifications, test measurements, and data acquisition and processing; Section 4 presents the test results under walking and shoveling conditions; Sections 5 and 6 are dedicated to the discussion and conclusions, respectively.

2. Analysis of Pure EWL

Due to the relatively small size of electric motors, their ability to start under load at zero speed, and the relative ease of arranging wires compared to drive shafts, the traditional system configuration of electric-driven loaders becomes more flexible. According to the different stages and tonnage sizes in the research of EWLs, the configurations primarily include the traditional type, the decoupled type for walking and working mechanisms, the dual-axle distributed drive fully decoupled type, and the independent four-wheel drive fully decoupled type, as is shown in Figure 1.

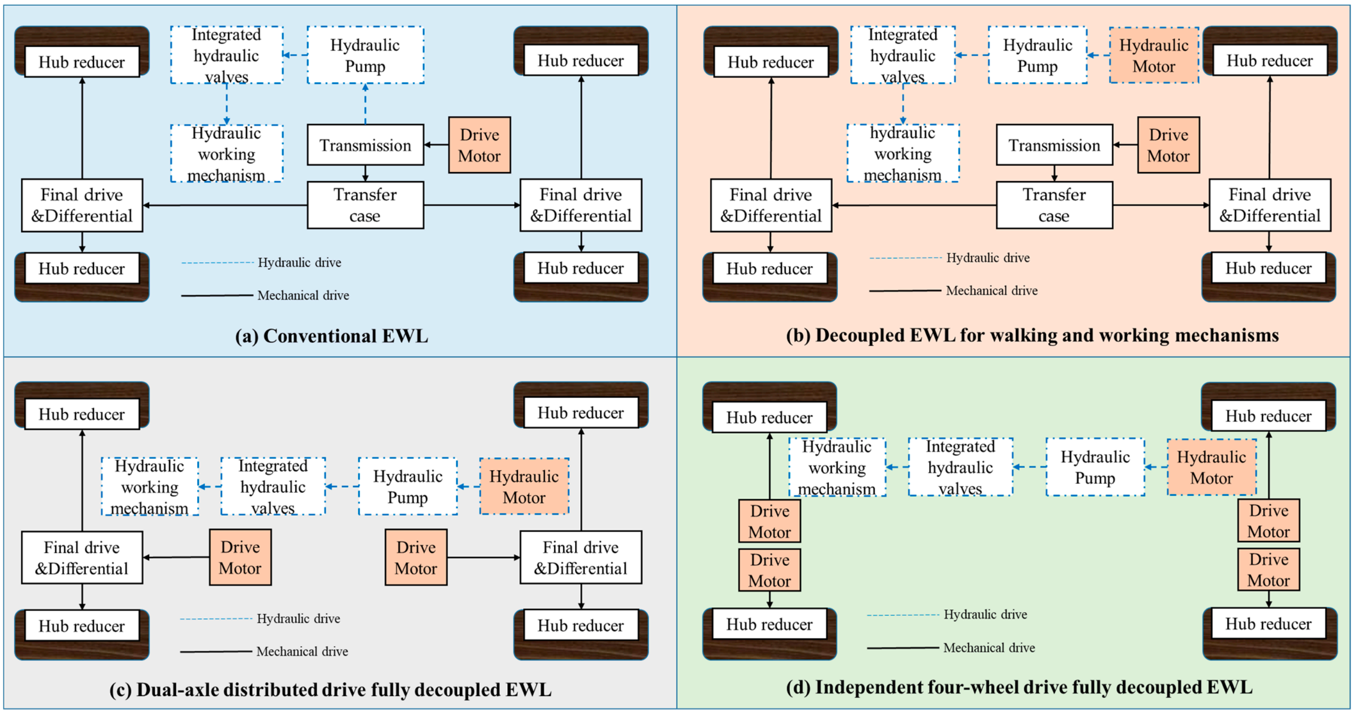

Figure 1. Typical schematic diagrams of EWL mechanism.

In a conventional EWL, a drive motor replaces the traditional diesel engine. This motor powers a mechanical transmission that drives both the front and rear axles, as well as the hydraulic pump, which supports the operation of the hydraulic working mechanism. As a result, the drive motor must be designed with high rated power and torque. In contrast, a decoupled EWL for walking and working mechanisms utilizes an additional motor specifically for driving the hydraulic pump, while the primary drive motor is dedicated solely to the walking system, similar to the configuration in a four-wheel-drive electric vehicle. Although this design increases the complexity of controlling the walking and hydraulic systems, it allows for easier selection and matching of the size and power of the two motors. The dual-axle distributed drive fully decoupled EWL, also known as the distributed electric drive wheel loader (DEWL) [24], utilizes one motor to drive the front drivetrain, another to drive the rear drivetrain, and a smaller motor to power the hydraulic system. This configuration allows the loader to operate in front-drive mode, rear-drive mode, or dual-drive mode, depending on the working conditions. This flexibility has attracted the attention of many researchers, as it can effectively reduce unnecessary parasitic power. In contrast, the independent four-wheel drive fully decoupled EWL is equipped with four motors, each driving one of the four wheels, along with an additional motor for the hydraulic system. This type is particularly suitable for super-heavy loaders that require significantly higher drive force during walking and shoveling operations. However, a major drawback is the difficulty in coordinating the control of the four drive motors, which can easily lead to the generation of parasitic power. Therefore, for a 5-ton EWL, the DEWL type is a suitable choice for application and further modification. This research aims to use a DEWL equipped with one motor to drive the front axle, and one motor to drive the rear axle.

3. Research Methods

3.1. Drive Theory of EWL

A WL is a type of off-road vehicle, classified as an articulated vehicle. Under travelling conditions, its driving principles are analogous to those of conventional road vehicles.

For an articulated vehicle composed of two separate bodies, the motion dynamics can be described by the equation presented in Equation (1) [25].

$$(m_1 + m_2)\ddot{x} = -F_{Lx} - (G_1 + G_2)sin\alpha + \sum_{j=1}^{n} X_j \tag{1}$$

where x is the longitudinal travel distance of a vehicle,m_1 and m_2 denote the mass of the front and rear bodies, respectively, while G_1 and G_2 represent the gravitational forces acting on the front and rear bodies. F_{Lx} refers to the atmospheric resistance in the longitudinal direction, α is the longitudinal slope angle of the road surface, and $\sum_{j=1}^{n} X_j$ signifies the sum of longitudinal forces acting on the axles.

If a WL is driven by a single axle, torque is generated on only the driving axle, while the other axle does not generate any torque if the friction is ignored. According to classic vehicle theory [25], the sum of resistance on the drive wheels can be calculated by Equation (2), while the drive force on the drive wheels can be calculated by Equation (3).

$$\mathrm{Z} = f_R G + c_x A \frac{\rho}{2} v_r^2 + \mathrm{G}(\mathrm{p} + \lambda \frac{\ddot{x}}{g}) \tag{2}$$

$$F_D = \frac{M_R i_o \eta}{r} \tag{3}$$

where Z represents the required driving force, the term f_R denotes the rolling resistance coefficient, while G represents the total gravitational force acting on the vehicle. The coefficient c_x is the atmospheric drag coefficient, A denotes the vehicle's windward area, ρ stands for air density, v_r is the vehicle speed, p indicates the road gradient, and λ is the vehicle's rotating mass factor. F_D stands for the drive force on the wheels, M_R indicates the drive torque generated by the power source, i_o is the transmission ratio from power source to drive wheel, η stands for mechanical efficiency, and r is the static radius of the drive wheel.

If the effect of velocity on rolling resistance is neglected, the power of the drive wheels on an axle can be expressed simply by Equation (4):

$$P_R = Z \frac{r}{R} v_r \tag{4}$$

where P_R is the power on the drive wheel, and R represents the dynamic radius of the tire during a sliding event. Generally, the ratio $\frac{r}{R}$ is approximately 1, indicating that wheel slip is typically neglected. However, if the sliding rate S is taken into account, P_R can be calculated using Equation (5):

$$P_R = Z \frac{r}{R} \times \frac{1}{1-S} v_r \tag{5}$$

Equation (5) demonstrates that the slip rate of the wheel significantly affects the vehicle's required power; if the wheel experiences complete sliding, the power required becomes infinite, rendering the vehicle unable to drive.

For an EWL, the drive torque on the wheels is entirely provided by the electric motor, achieving equilibrium when Z equals F_D. Therefore, a high transmission ratio and substantial motor power are beneficial for increasing the drive force.

3.2. Drive Force Requirement Analysis

A WL needs to overcome not only the driving resistance, but more importantly, the insertion resistance, which is much higher than driving resistance. Cao et al. [26] analyzed the insertion resistance of an engine drive WL with experimental data. Wang et al. [27], Madau et al. [28] and Chen et al. [29] have discussed the insertion resistance of WL. As presented in Equation (6) [30], the insertion resistance is calculated.

$$F_{Ins} = 9.8 \cdot \Lambda_1 \cdot \Lambda_2 \cdot \Lambda_3 \cdot \Lambda_4 \cdot W_B \cdot D^{1.25} \tag{6}$$

where F_{Ins} is the insertion resistance; Λ_1 represents the influence coefficient of material pile looseness; Λ_2 is the influence coefficient of material type; Λ_3 denotes the influence coefficient of pile shape and height; Λ_4 stands for the influence coefficient of the bucket; W_B is the width of the bucket; D is the insertion depth.

Therefore, the total resistance of a WL is calculated by Equation (7), where F_{Req} represents the drive force a WL requires when working in a shoveling condition. Assuming that the WL is operating in a shoveling condition on level terrain, where both atmospheric resistance and accelerating resistance can be neglected due to the WL's approach-zero speed, Equation (7) can be simplified to yield Equation (8).

$$F_{Req} = 9.8 \cdot \Lambda_1 \cdot \Lambda_2 \cdot \Lambda_3 \cdot \Lambda_4 \cdot W_B \cdot D^{1.25} + f_R G + c_x A \frac{\rho}{2} v_r^2 + \mathrm{G}(\mathrm{p} + \lambda \frac{\ddot{x}}{g}) \tag{7}$$

$$F_{Req} = 9.8 \cdot \Lambda_1 \cdot \Lambda_2 \cdot \Lambda_3 \cdot \Lambda_4 \cdot W_B \cdot D^{1.25} + f_R G \tag{8}$$

For the gravel material pile, Λ_1 equals 0.75, Λ_2 equals 0.12, Λ_3 is 1.1, Λ_4 is 1.4, while for the sand pile, Λ_1 decreases to 0.5, Λ_2 to 0.1, and Λ_3 and Λ_4 remained unchanged. In this study, the tested EWL has a weight of 17,300 kg, a rated load capacity of 5300 kg, and a bucket width of 299 cm. The rolling resistance coefficient ranges from 0.20 to 0.25 on dry gravel pavement, whereas it varies between 0.1 and 0.3 on dry sand pavement. Table 1 shows the comparison of resistance at insertion depths for gravel and sand piles. For the gravel material pile, the influence coefficients are as follows: Λ_1 is 0.75, Λ_2 is 0.12, Λ_3 is 1.1, and Λ_4 is 1.4. In contrast, for the sand pile, Λ_1 decreases to 0.5, Λ_2 is reduced to 0.1, while Λ_3 and Λ_4 remain unchanged. In this study, the tested EWL has a weight of 17,300 kg, a rated load capacity of 5300 kg, and a bucket width of 293 cm. The rolling resistance coefficient ranges from 0.20 to 0.25 on dry gravel pavement, whereas it varies between 0.1 and 0.3 on dry sand pavement. Table 1 presents a comparison of resistance at various insertion depths for gravel and sand piles.

Table 1. Insert resistance and rolling resistance comparison in various shoveling conditions.

Pile Material	Insert Depth (cm)	50	60	70	80	90	100
Dry gravel	Insertion resistance (kN)	52.91	66.45	80.58	95.21	110.32	125.85
	Rolling resistance (kN)	34.6–43.25					
Dry sands	Insertion resistance (kN)	29.39	36.92	44.76	52.90	61.29	69.91
	Rolling resistance (kN)	17.3–51.9					

The results of a comparison between the calculated and measured insertion resistance for gravel and sand piles indicate that the actual insertion resistance is higher than the calculated values in most cases [29]. This further proves that a WL demands more power to work.

In Figure 2, the speed and torque curves for the tested EWL under free shoveling conditions are illustrated. Two motors independently drive the WL through the front and rear axles. Each drivetrain features an identical transmission ratio of 22.85, an overall mechanical efficiency of 95%, and a wheel radius of 0.805 m. During this test period, a positive value for the front motor speed or torque indicates that the EWL is moving forward, while a positive value for the rear motor speed or torque indicates backward movement, due to the configuration of the data acquisition system.

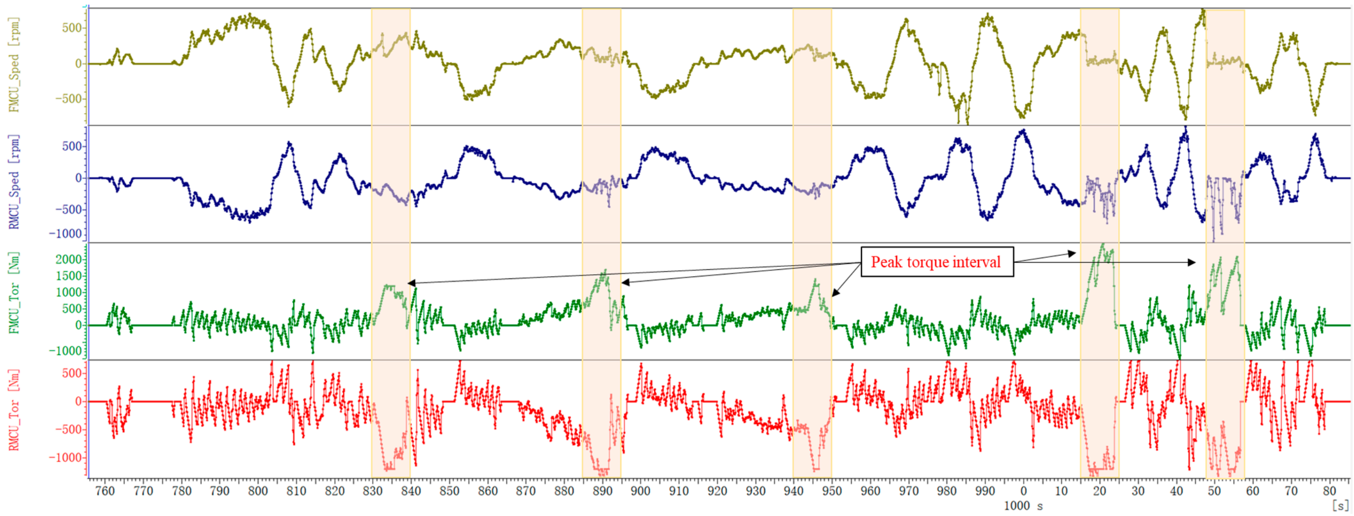

Figure 2. Speed and torque for two drive motors in shoveling condition.

As shown in Figure 2, the relative maximum torques of the front and rear motors occurred six times, within the time intervals of 830–840 s, 885–895 s, 940–950 s, 1015–1025 s, and 1048–1058 s, the last of which contains two peak torques. Among these six instances, the highest torque was observed between 1015 s and 1025 s, where the front motor reached a maximum torque of 2481 Nm, and the rear motor reached a maximum torque of 1854 Nm. According to Equation (2), the sum drive force F_{sum} on wheels connected to the front axle and the rear axle can be calculated and listed in Table 2, where F_{FD} and F_{RD} represent the drive force of the front wheels and the rear wheels, respectively, and T_{FD} and T_{RD} stand for the torques generated by the front and the rear motors, respectively.

Table 2. Peak drive force on wheels in shoveling condition.

Time Range (s)	830–840	885–895	940–950	1015–1025	1050–1052	1054–1058
T_{FD} (Nm)	1225	1656	1412	2481	2069	2093
F_{FD} (kN)	33.03	44.66	38.08	66.90	55.79	56.44
T_{RD} (Nm)	1213	1483	1200	1531	1729	1459
F_{RD} (kN)	32.71	39.99	32.36	41.28	46.62	39.34
F_{sum} (kN)	65.74	84.65	70.43	108.19	102.42	95.78

According to the calculated values presented in Table 1, the EWL can overcome a maximum resistance of 51.9 kN under running conditions. In this study, the maximum tractive force measured during the shoveling tests was 108 kN, which clearly satisfies the required performance. Additionally, both the front and rear motors are PMSMs, each with a maximum torque of 3000 Nm. Theoretically, if road adhesion is sufficient, the WL's tractive force could reach up to 160 kN.

Assuming that a WL is operating on level terrain, the required driving force needed during the process can be expressed as Equation (9), where φ is the adhesion coefficient.

$$F_{Req} \approx \begin{cases} f_R G, & S < 1,\ D = 0 \\ f_R G + F_{Ins}, & S < 1,\ D > 0 \\ \varphi G, & S = 100\% \end{cases} \tag{9}$$

3.3. Structure Modification of Front Axle

From the analysis of the tractive force requirements mentioned above, it is evident that the force provided by the motors must not only overcome the driving resistance but also the penetration resistance encountered during shoveling. If complete tire slippage occurs, the reaction force provided by the ground is limited by the available traction. The analysis of Figure 2 and Table 2 indicates that the maximum tractive forces of the front and rear motors do not occur simultaneously. Moreover, despite having identical transmission ratios and tire sizes, the motors driving the front and rear axles exhibited inconsistent rotational speeds during shoveling. Data from a 22 s shoveling period are extracted for further analysis, as shown in Figure 3.

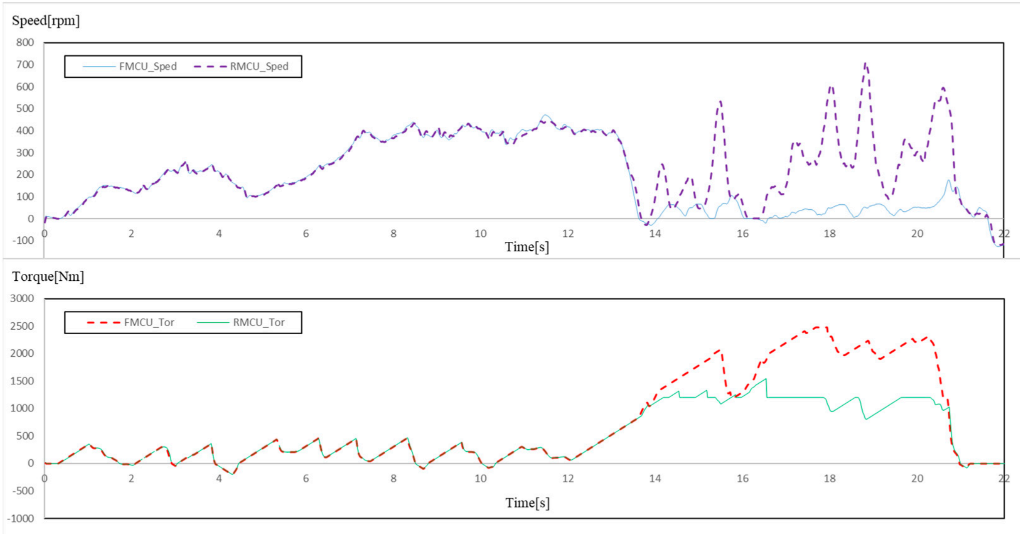

Figure 3. Tire sliding during shoveling process.

The speed and torque curves of the drive motors in Figure 3 indicate that the speeds and torques of both motors remain closely aligned from 0 to 14 s. This suggests that the torque generated by the traction motors is evenly distributed during this initial period. However, as the torques on both motors increase, the torque on the front motor begins to exceed that of the rear motor between approximately 14 and 21 s. Simultaneously, the speed of the rear motor surpasses that of the front motor. This phenomenon is caused by the forward shift in the WL's center of gravity [31], as the bucket experiences increased vertical force from the material pile.

In such cases, the rear wheels slide from the insufficient adhesion force, due to the vertical pressure decreasing on the rear axle. Therefore, given the operational characteristics of WLs, it is possible to design the front drive axle to deliver a greater portion of the total tractive force, while the rear motor can provide relatively less, as long as the overall tractive force requirement is met. The total tractive force can be calculated using Equation (10).

$$F_{Tr} = \frac{T_F i_{OF} \eta_F}{r_F} + \frac{T_R i_{OR} \eta_R}{r_R} \tag{10}$$

where F_{Tr} represents the overall traction force of the EWL; T_F and T_R are the torques generated by the front and rear motors, respectively; i_{OF} and i_{OR} are the overall transmission ratios of the front and rear drivetrains, respectively; η_F and η_R denote the mechanical efficiencies of the front and rear drivetrains, respectively; r_F and r_R are the static radii of the front and rear tires.

According to Equation (10), the transmission ratio of the front drivetrain can be increased to enhance the tractive force on the front wheels. If i_{OF} is doubled, the tractive force on the front wheels can also be doubled. However, this increase comes with a limitation; the velocity of the EWL will be reduced to half of its previous value [32].

In this study, a front drivetrain with a transmission ratio of 44.05 replaced the original one with a transmission ratio of 22.85. Thus, an SRM with a rated torque of 955 Nm is introduced as the drive motor. Tables A1–A3 present the test data of the SRM before it was matched to the front drive motor. The featured parameters of the SRM are listed in Table 3.

Table 3. Parameters of the SRM.

Items	Parameters	Items	Parameters
Rated torque	955 Nm	Peak torque	3200 Nm
Rated voltage	620 VDC	Rated power	100 kW
Rated speed	1000 rpm	Mass	490 kg
Max. speed	3000 rpm	Efficiency	93.25%

For comparison, no changes were made to the rear drivetrain; the rear transmission ratio remains 22.85, and the rear drive motor is the PMSM, with its featured parameters listed in Table 4.

Table 4. Parameters of the rear drive motor (PMSM).

Items	Parameters	Items	Parameters
Rated torque	1200 Nm	Peak torque	3200 Nm
Rated voltage	540 VDC	Rated power	120 KW
Rated speed	955 rpm	Mass	240 Kg
Max. speed	3000 rpm	Efficiency	95%

3.4. Test Methods and Procedures

Given the modifications to the drivetrain, drive tests under walking and shoveling conditions should be conducted to validate the drive performance of the SRM on the improved EWL. Figure 4a shows the walking experiment process for the EWLs in this study. First, the original EWL is driven by the front PMSM at speeds of 200 rpm, 400 rpm, and 600 rpm. Next, the same EWL is driven by the rear PMSM under the same conditions. The modified EWL then undergoes the same series of tests, with the key difference being that the front drive motor is replaced by an SRM. It is important to emphasize that each of the tests mentioned above should be repeated three times. Upon completing these procedures, the average drive force, average drive power, and average drive efficiency are calculated and compared between the original and modified EWLs to assess the improvements achieved by incorporating the SRM.

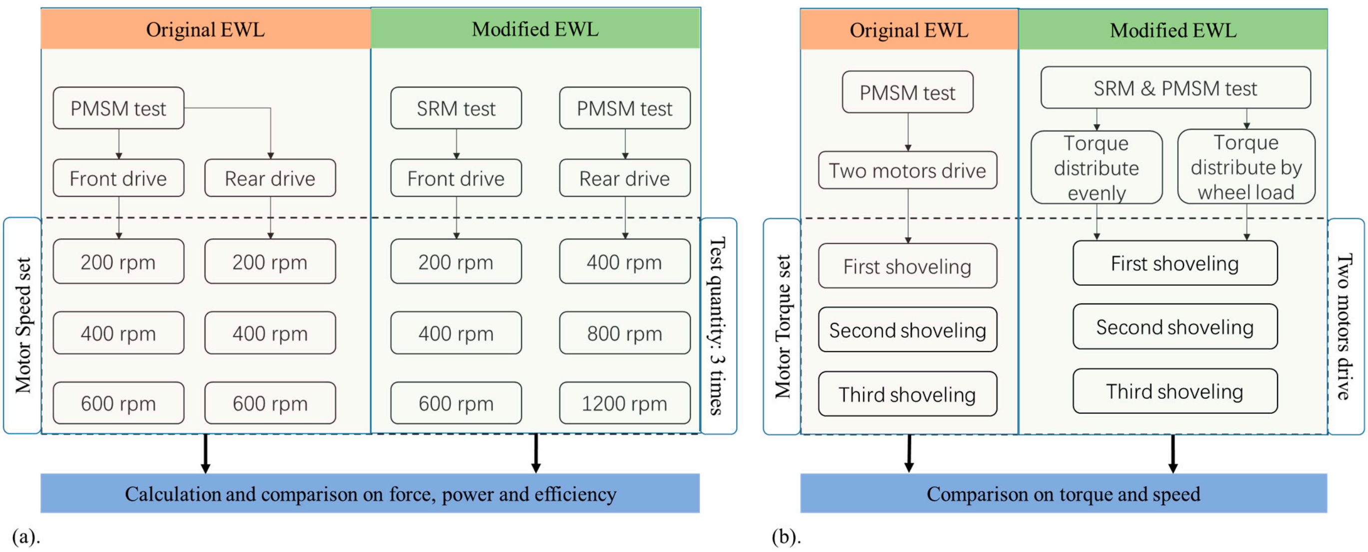

Figure 4. Test program for EWL in (**a**) walking conditions and (**b**) shoveling conditions.

It should also be noted that when any of the motors is designated as the drive motor, its speed should be set to specific limits, such as 200 rpm, 400 rpm, or 600 rpm. However, in the modified EWL, because the transmission ratio of the front drivetrain is nearly twice that of the rear, if the SRM is used as the drive motor, the speeds are set to 400 rpm, 600 rpm, and 1200 rpm to maintain a velocity similar to that achieved when driven by the rear motor.

The other series of tests is conducted under shoveling conditions to validate the drive performance of the SRM on the modified EWL. However, the drive performance during the shoveling process is influenced by the drive torque distribution strategy applied to the EWL. Unlike the walking tests, the shoveling test cannot be performed using only the front or rear motor. If only the rear motor is used, the rear drive wheels may lift off the ground, preventing the EWL from moving forward. Conversely, if only the front motor is used, the EWL may lack sufficient drive force. The shoveling test procedure is shown in Figure 4b.

For the newly developed EWL, two distinct torque distribution control strategies were applied to evaluate their performance during shoveling operations [33]. The first approach allocates equal drive force to both the front and rear wheels, as dictated by the VCU based on accelerator pedal input. This control method is illustrated in Figure 5a. The second approach distributes torque according to the load on each wheel, with the front wheel load corresponding to the hydraulic pressure in the base cylinder of the tilt. In both strategies, the combined torque from the front and rear motors matches the required torque as determined by the accelerator pedal's position. This control strategy is depicted in Figure 5b.

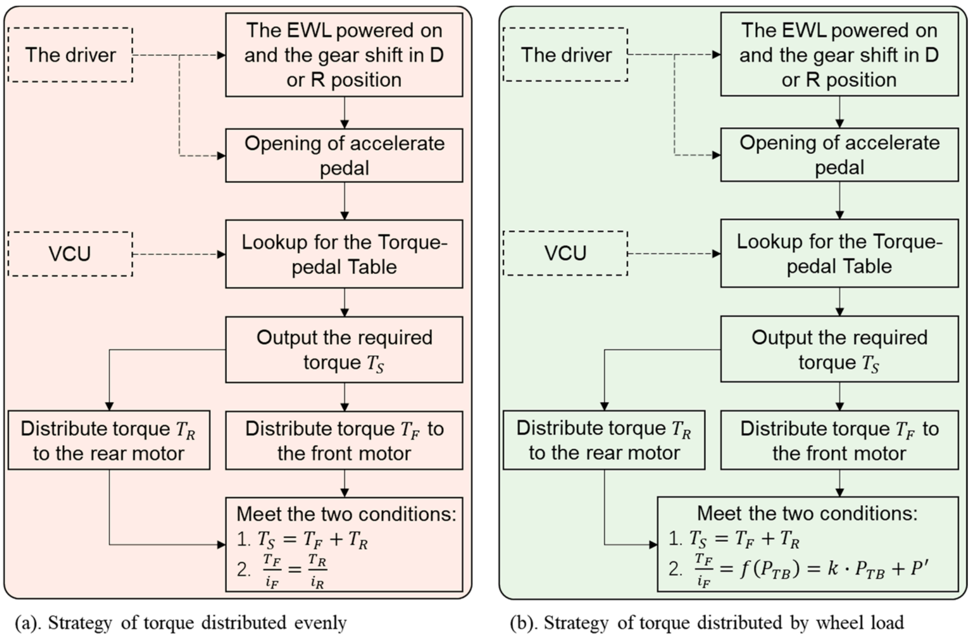

Figure 5. Torque distribution control strategies in shoveling tests [33].

3.5. Data Acquisition and Processing

Typically, onboard data are transmitted via the vehicle control unit's CAN bus. By connecting a CANDTU data acquisition box to the CAN bus, data from the vehicle in operation can be recorded. However, the recorded data are not directly readable by humans and need to be converted into '.asc' format using CANDTU-200UR software, as illustrated in Figure 6. The baud rate for data acquisition is set to 100 Hz, that is, the data are recorded every 10 milliseconds.

The converted file can be opened with Vector CANoe software (version 9.0), but before reading the data, the signal names must be edited. Each data point has a unique address code; for example, one set of information from the front motor has the address code 18ffb1f0. By combining this address code with the communication protocol, signal parameters can be defined, allowing the data to be read, as illustrated in Figure 7.

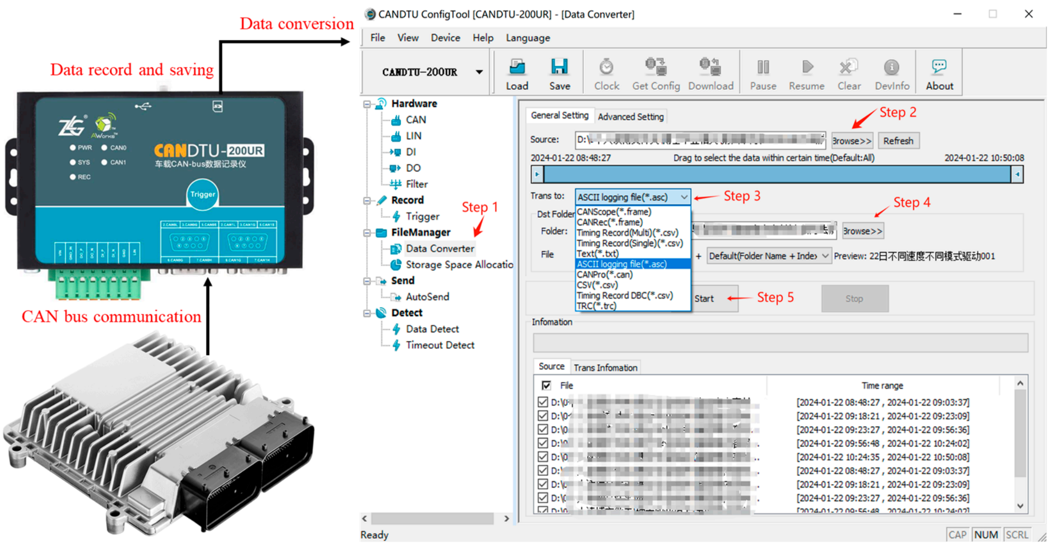

Figure 6. Settings of data acquisition tool CANDTU-200R.

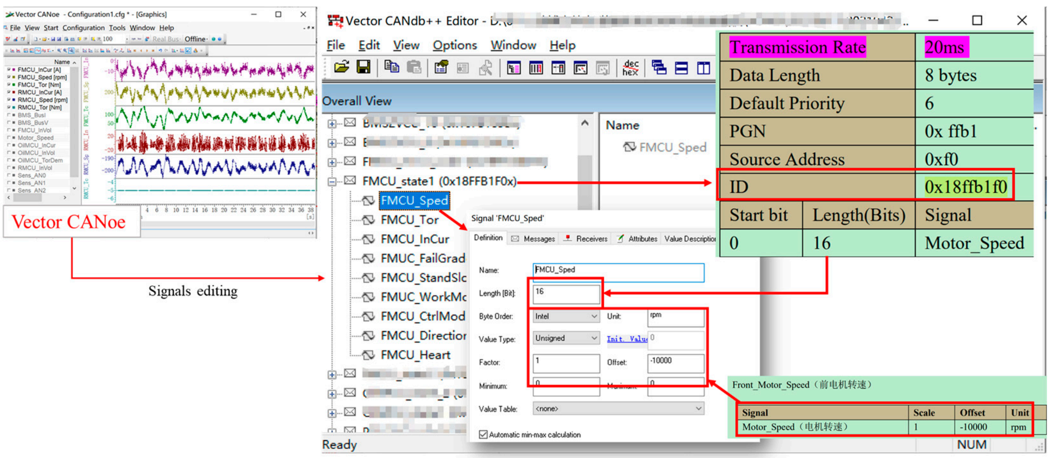

Figure 7. Data processing software CANoe.

4. Results

4.1. Result of Walking Condition

Figure 8 presents the curves of the two PMSMs, where the front motor is designated as the drive motor at a speed of 200 rpm under walking conditions. It is evident that the torque fluctuation is unstable during the process. In the figure, FMCU_InCur represents the input current of the front motor's control unit, FMCU_Sped denotes the speed of the front motor, and FMCU_Tor indicates the torque of the front motor. Similarly, RMCU_InCur stands for the input current of the rear motor's control unit, RMCU_Sped for the speed of the rear motor, and RMCU_Tor for the torque of the rear motor. The raw data values are displayed as positive or negative to differentiate between the front and rear motors; for example, the speed of the rear motor is negative even though the rear wheel rotates forward. After further processing, the data are presented in a standard format in Appendix B.

The average current, average torque, and average output power, as shown in Table 5, are calculated based on the data from the curves in Figures A1–A3. The parameters presented in Table 6 are calculated based on Figures A4–A6. Here, $\overline{I}_{FM}$ stands for the average current of the front motor with the unit of Ample, $\overline{T}_{FM}$ denotes the average torque of the front motor with the unit of Nm. In the original EWL, the front and rear transmission ratios are identical. As a result, when one PMSM is selected as the drive motor, the other PMSM is passively driven at the same speed as the drive motor, which can be observed in the curve figures. Consequently, the speed of the dragged PMSM in both F-drive and R-drive modes is not presented in Table 5 or Table 6. Here, F-drive refers to the EWL being driven solely by the front motor, while R-drive indicates that the EWL is driven solely by the rear motor.

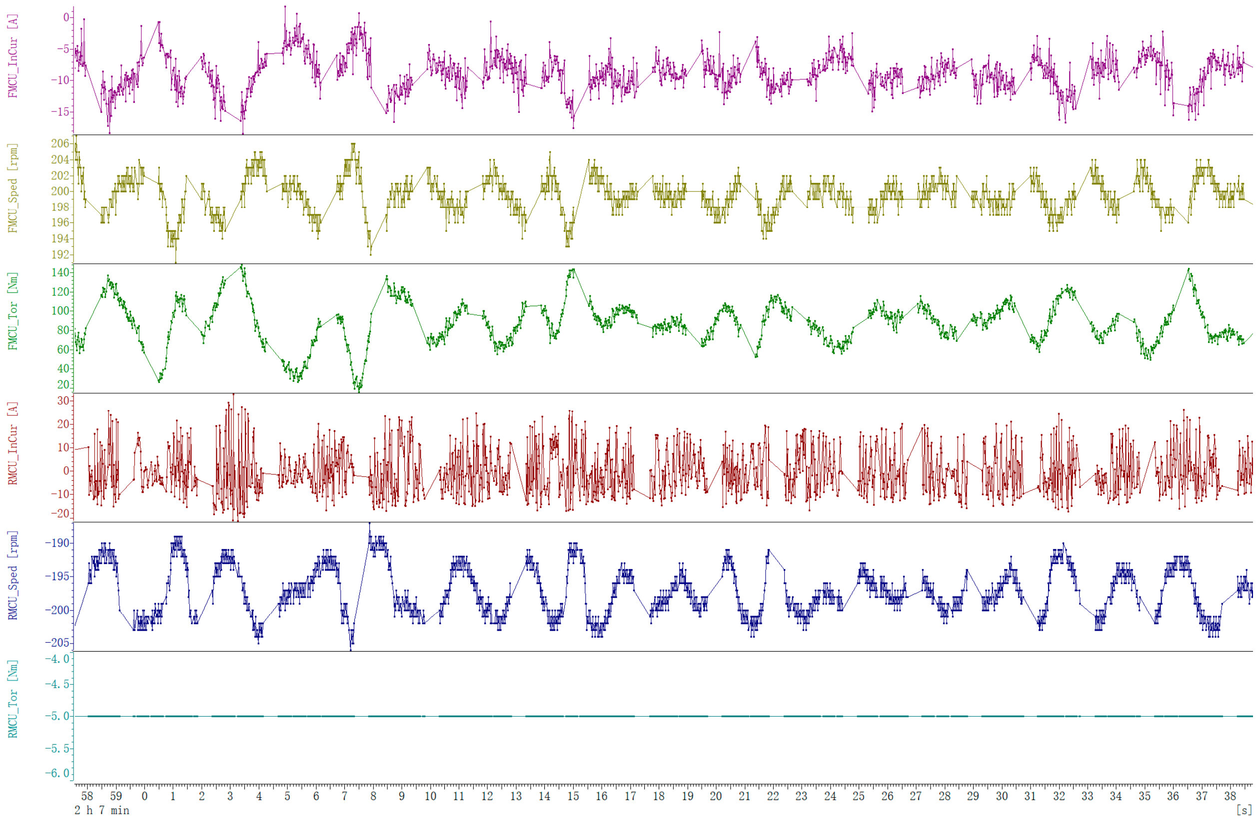

Figure 8. Curves of motors in F-drive mode at speed of 200 rpm in walking condition.

Table 5. Calculated data for the original EWL tested in F-drive mode under walking conditions.

Items	200 rpm			400 rpm			600 rpm		
$\overline{T}_{FM}$ (Nm)	347.51	327.82	331.30	346.75	338.91	371.76	390.54	345.74	344.88
$\overline{P}_{FM}$ (kW)	7.28	6.87	6.94	14.52	14.20	15.57	24.54	21.72	21.67

Table 6. Calculated data for the original EWL tested in R-drive mode under walking conditions.

Items	200 rpm			400 rpm			600 rpm		
$\overline{T}_{RM}$ (Nm)	229.77	230.10	230.22	262.44	246.46	250.85	271.66	270.00	267.54
$\overline{P}_{RM}$ (kW)	4.81	4.82	4.82	10.99	10.32	10.51	17.07	16.96	16.81

Compared to the tests on the original EWL, the data for the modified EWL include the speed of the passive drive motor, as shown in Tables 7 and 8, which are drawn from Figures A7–A12. In Table 7, the SRM is the drive motor, with test speeds set to 400 rpm, 800 rpm, and 1200 rpm, corresponding to 200 rpm, 400 rpm, and 600 rpm of the rear motor. However, Table 7 demonstrates that the actual corresponding speeds are approximately 208 rpm, 415 rpm, and 623 rpm. In Table 8, the PMSM is the drive motor, with test speeds set to 200 rpm, 400 rpm and 600 rpm, which is similar to the test on the original EWL.

Table 7. Calculated data for the modified EWL tested in F-drive mode under walking conditions.

Items	400 rpm			800 rpm			1200 rpm		
$\overline{T}_{FM}$ (Nm)	155.31	137.27	146.5	177.0	169.88	166.73	193.8	186.43	184.98
$\overline{n}_{RM}$ (rpm)	208.04	207.56	208.05	415.69	415.68	415.8	623.46	622.63	623.51
$\overline{P}_{FM}$ (kW)	6.51	5.75	6.14	14.83	14.23	13.97	24.35	23.43	23.24

Table 8. Calculated data for the modified EWL tested in R-drive mode under walking conditions.

Items	200 rpm			400 rpm			600 rpm		
$\overline{T}_{RM}$ (Nm)	223.52	216.94	209.06	250.21	238.93	233.49	259.13	254.57	251.79
$\overline{n}_{FM}$ (rpm)	381.4	382.18	382.44	765.67	764.84	763.17	1146.79	1147.06	1146.66
$\overline{P}_{RM}$ (kW)	4.68	4.54	4.38	10.48	10.01	9.78	16.28	15.99	15.82

4.2. Result of Shoveling Condition

Figure 9 displays the test curves for the original EWL, highlighting four stages of shoveling operations. The light green shaded areas indicate the most prominent shoveling phases, which typically start with zero torque, gradually increase, and then gradually decrease, ending at zero torque.

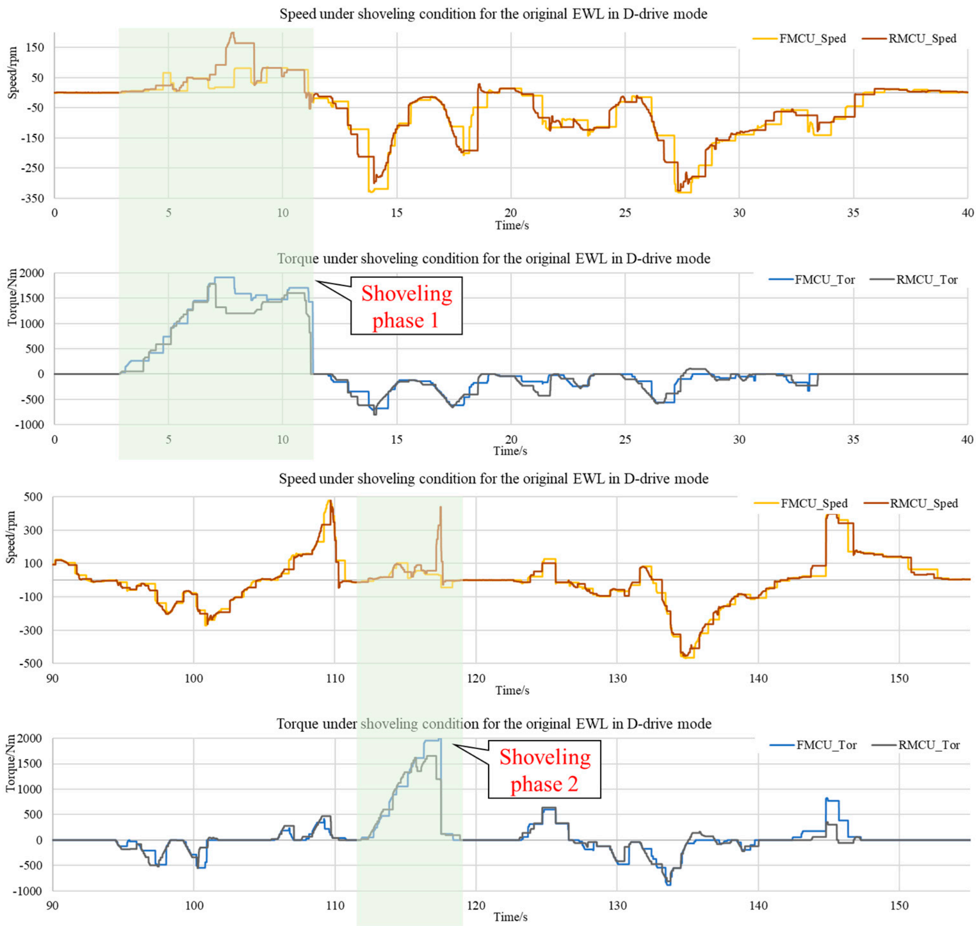

(a)

(b)

Figure 9. *Cont.*

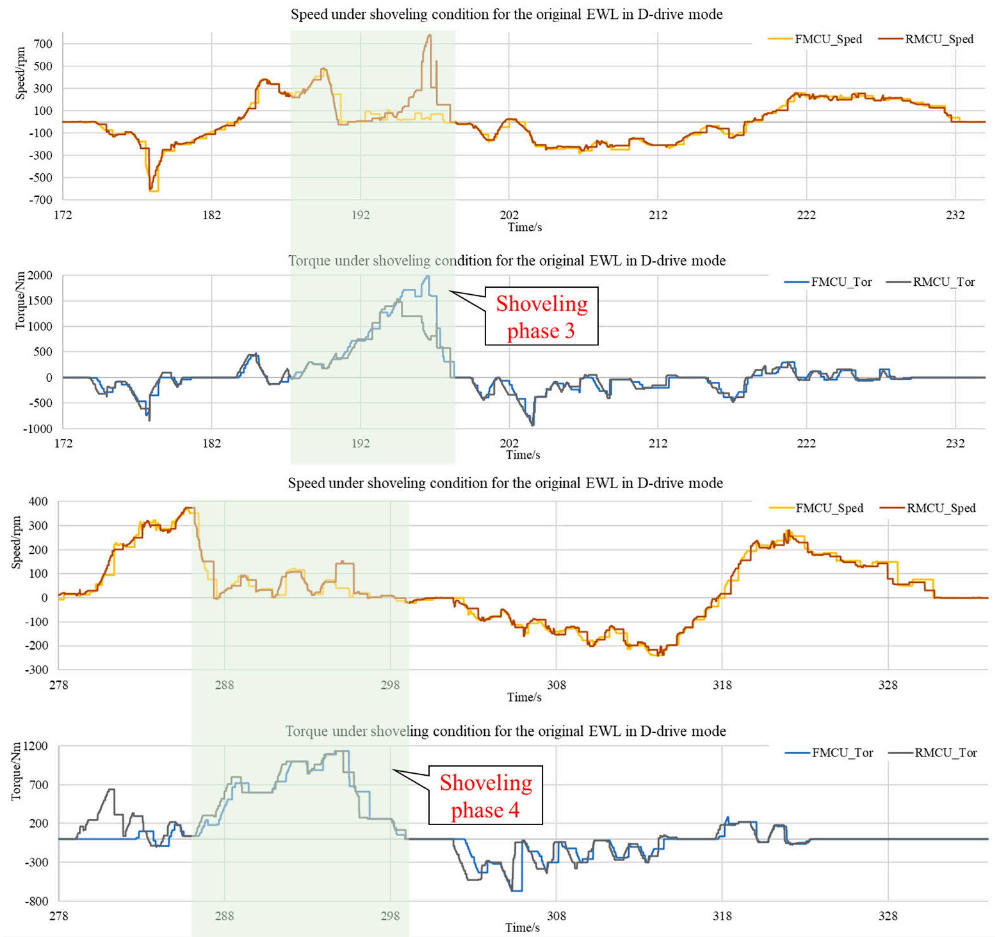

(**c**)

(**d**)

Figure 9. The speed and torque curves of continuous shoveling test for the original EWL.

The first shoveling phase occurs from approximately 2.84 s to 11.45 s, during which the maximum torque of the front motor reaches 1910 Nm. Within this time frame, as shown in Table 9, the minimum torque of the rear motor is 1200 Nm. The parameters of the other three shoveling stages are also listed in Table 9, where T_{FM_max} represents the maximum torque of the front motor during a prominent shoveling stage, ΔT_{max} denotes the largest difference between the maximum torque of the front and rear motors during the period when the front motor's maximum torque is achieved, and CTP T_{RM_min} indicates the minimum torque of the rear motor at the corresponding time.

Table 9. Statistic data of the original EWL under shoveling test in 4 stages.

Items	Start Time (s)	End Time (s)	T_{FM_max} (Nm)	ΔT_{max} (Nm)	CTP T_{RM_min} (Nm)
Stage 1	2.84	11.45	1910	710	1200
Stage 2	111.84	119.24	2000	800	1200
Stage 3	187.41	198.54	1986	1213	773
Stage 4	286.16	299.11	1136	861	275

For the shoveling test on the modified EWL, two series of tests were conducted. Figure 10 illustrates the speed and torque curves with evenly distributed drive force, depicting three shoveling stages. In this set of tests, the shoveling stages last about 15 s. A notable feature observed is that the torque of the rear motor decreases from a high value to zero within a very short time.

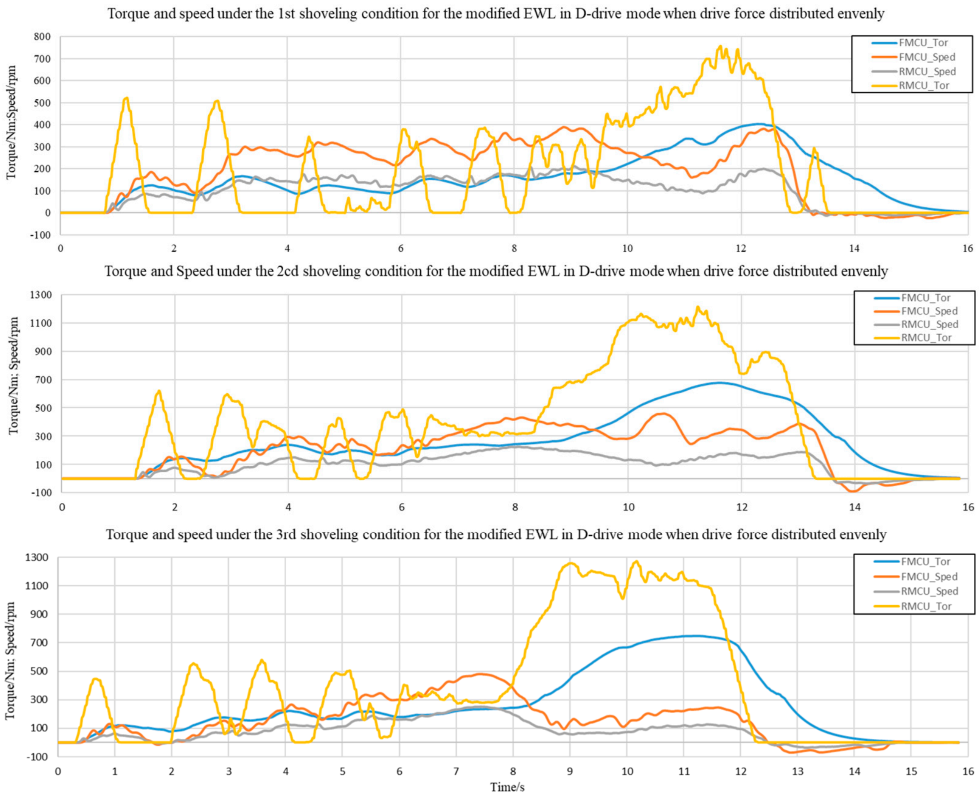

Figure 10. The speed and torque curves of three shoveling tests for the modified EWL under evenly distributed drive force strategy.

For the shoveling test with drive force distributed according to wheel load, the results for speed and torque of the motors are shown in Figure 11. In this set of tests, although the overall stage time appears longer, the actual shoveling duration is approximately 14 s.

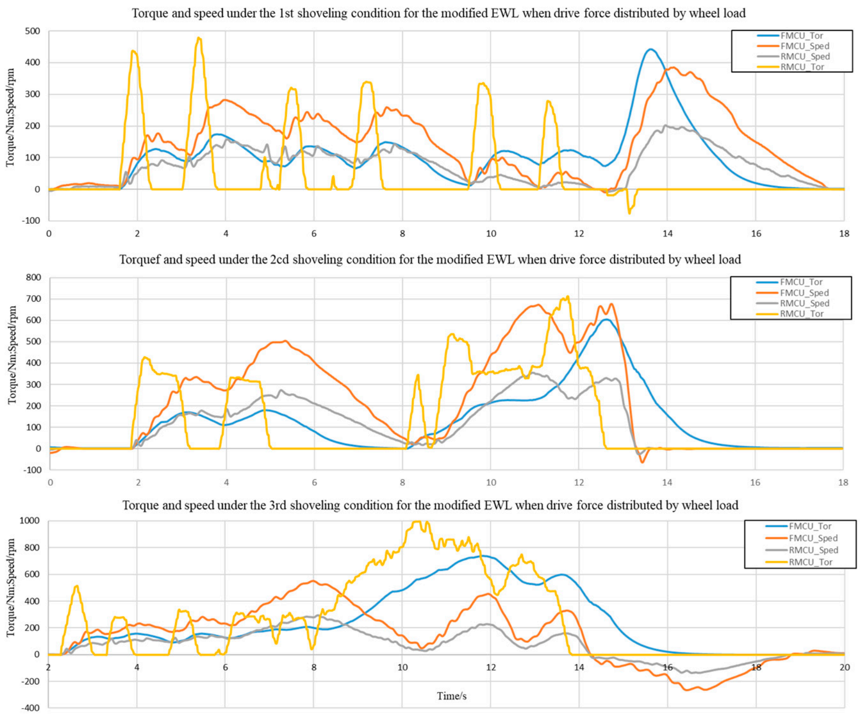

Figure 11. The speed and torque curves of three shoveling tests for the modified EWL under drive force distributed by wheel load strategy.

To compare the two shoveling tests for the modified EWL, Table 10 lists the maximum torque of the front and rear motors, as well as the corresponding calculated torque on the drive wheels. Assuming an overall mechanical efficiency of 95% for both the front and rear drivetrains, the torque on the drive wheels can be computed using Equation (11), where T_F and T_R represent the torques on the front and rear drive wheels, respectively. The values for i_{OF} and i_{OR} are 44.05 and 22.85, respectively.

$$\begin{cases} T_F = T_F \cdot i_{OF} \cdot \eta_F \\ T_R = T_R \cdot i_{OR} \cdot \eta_R \end{cases} \tag{11}$$

Table 10. Statistic data of the original EWL under shoveling test with two strategies.

Control Method	Items	T_{FM_max} (Nm)	T_{RM_max} (Nm)	T_F (Nm)	T_R
Torque distributed evenly	Stage 1	404.2	757	16,915	16,433
	Stage 2	676	1215	28,289	26,375
	Stage 3	748	1273	31,302	27,634
Torque distributed by wheel load	Stage 1	442.2	479	18,505	10,398
	Stage 2	605.2	712	25,326	15,456
	Stage 3	737.7	995	30,871	21,599

5. Discussion

5.1. Comparison of Drive Performance in Walking Condition

For the original EWL, when the front motor is used as the drive motor, the average torque of the three tests at 200 rpm is 335.54 Nm with an average power of 7.03 kW. At 400 rpm, the average torque and power increase to 352.47 Nm and 14.76 kW, respectively. At 600 rpm, these values rise further to 360.39 Nm and 22.64 kW. These data indicate that power consumption increases with speed. Similarly, when the rear motor is assigned as the drive motor, the average torque at 200 rpm, 400 rpm, and 600 rpm is 230.03 Nm, 253.25 Nm, and 269.73 Nm, respectively, with average power values of 4.82 kW, 10.61 kW, and 16.95 kW. Table 11 summarizes the average power in walking conditions. This pattern of increasing power consumption with speed is consistent with that observed when the front motor is used.

Table 11. Average power consumption of three tests on the original EWL under walking condition.

Motor Speed (rpm)	Average Power (kW)	Average Power (kW)	Ratio of Power in R-Drive to Power in F-Drive (%)
200	7.03	4.82	68.56
400	14.76	10.61	71.88
600	22.64	16.95	74.87
Note	F-drive mode	R-drive mode	\

It is evident that all average power values in F-drive mode are greater than those in R-drive mode. At motor speeds of 200 rpm, 400 rpm, and 600 rpm, power consumption in R-drive mode accounts for 68.56%, 71.88%, and 74.87% of that in F-drive mode, respectively. This indicates that the rear motor consumes less power than the front motor when used as the drive motor at a given speed, and more importantly, it provides better drive performance at lower speeds.

For the modified EWL, when the assigned SRM is used in F-drive mode, the average torque for the three tests is 146.36 Nm, 171.20 Nm, and 188.40 Nm at speeds of 400 rpm, 800 rpm, and 1200 rpm, respectively. And the average power for the three tests is 6.13 kW, 14.34 kW, and 23.67 kW at speeds of 400 rpm, 800 rpm, and 1200 rpm, respectively. This group of data also shows that the torque and power of the SMR increase with the speed. Additionally, in the R-drive mode, when the PMSM is assigned as the drive motor, the average torque at 200 rpm, 400 rpm, and 600 rpm is 216.5 Nm, 240.88 Nm, and 255.16 Nm, respectively, with average power values of 4.53 kW, 10.09 kW, and 16.03 kW. This rule is similar to that of the test on the original EWL. Table 12 summarizes the average torque and power of the test on the modified EWL in walking conditions.

Table 12. Average power consumption of three tests on the modified EWL under walking condition.

Front Motor Speed (rpm)	Average Rear Speed (rpm)	Average Power (kW)	Rear Motor Speed (rpm)	Average Front Speed (rpm)	Average Power (kW)	Ratio of Power in R-Drive to Power in F-Drive (%)
400	207.88	6.13	200	382.01	4.53	73.90%
800	415.72	14.34	400	764.56	10.09	70.35%
1200	623.20	23.67	600	1146.84	16.03	67.72%
	F-drive mode			R-drive mode		\

When testing the modified EWL, it is evident that all average power values in F-drive mode are higher than those in R-drive mode. Power consumption in R-drive mode accounts for 73.90%, 70.36%, and 67.72% of that in F-drive mode, at rear motor speed of 200 rpm/208 rpm, 400 rpm/416 rpm and 600 rpm/623 rpm. This indicates that the rear motor consumes less power than the front motor, yet it delivers better drive performance at higher speeds.

From the above discussion, it can be concluded that if the rear motor is set as the drive motor on an EWL, it will consume less power compared to when the front motor is used as the drive motor. Additionally, if a PMSM is assigned as the front drive motor, the rear drive motor performs better at lower speeds in a single-axle drive mode. Conversely, if an SRM is assigned as the front drive motor with an approximately double transmission ratio compared to the rear drivetrain, the rear drive motor performs better at higher speeds.

5.2. Comparison of Drive Performance in Shoveling Condition

In the shoveling test on the original EWL, the first three stages exhibit heavier shoveling loads compared to the fourth stage. As shown in Table 9, the maximum torque of the front motor reaches 1910 Nm, 2000 Nm, and 1986 Nm during the first, second, and third tests, respectively. During the periods when these maximum torques occur, the corresponding minimum torque of the rear motor is 1200 Nm, 1200 Nm, and 773 Nm. Consequently, the largest torque difference between the front and rear motors is 1213 Nm, which occurs during the third stage.

Another common feature of the four shoveling stages presented in Figure 9 is that the maximum torque of the front motor consistently exceeds that of the rear motor. Additionally, the speed curves in Figure 9 indicate that rear-wheel slippage occurred in all tested stages, suggesting insufficient adhesion between the rear wheels and the ground surface.

In the shoveling test on the modified EWL, each group of tests under two drive torque distribution strategies was conducted three times.

For the tests with evenly distributed torque, the maximum torque of the front motor was 404 Nm, 676 Nm, and 748 Nm, respectively, while the corresponding maximum torque of the rear motor was 757 Nm, 1215 Nm, and 1273 Nm. Although the raw data show significant differences, when recalculated as the corresponding torque on the drive wheels, the maximum torque on the front drive wheels was 16,915 Nm, 28,289 Nm, and 31,302 Nm, respectively, and the torque on the rear wheels was 16,433 Nm, 26,375 Nm, and 27,634 Nm. The difference rate of driving force generated on the front and rear wheels is calculated to be 2.85%, 6.77%, and 11.72%, respectively. These adjusted values show that the torque on the front and rear wheels is much closer, aligning with the torque distribution strategy. Compared to the tests on the original EWL, the torques of the front motor in this group of shoveling tests are much lower, but the drive force can reach 22.11 kN, 36.97 kN and 40,91 kN in each test, which can be derived from Figure 12. It can also be concluded from Figure 12 that the yellow shaded area represents the outstanding shoveling phases, where the rear drive force reached its maximum value earlier, but the maximum values of the front drive forces reached later are higher.

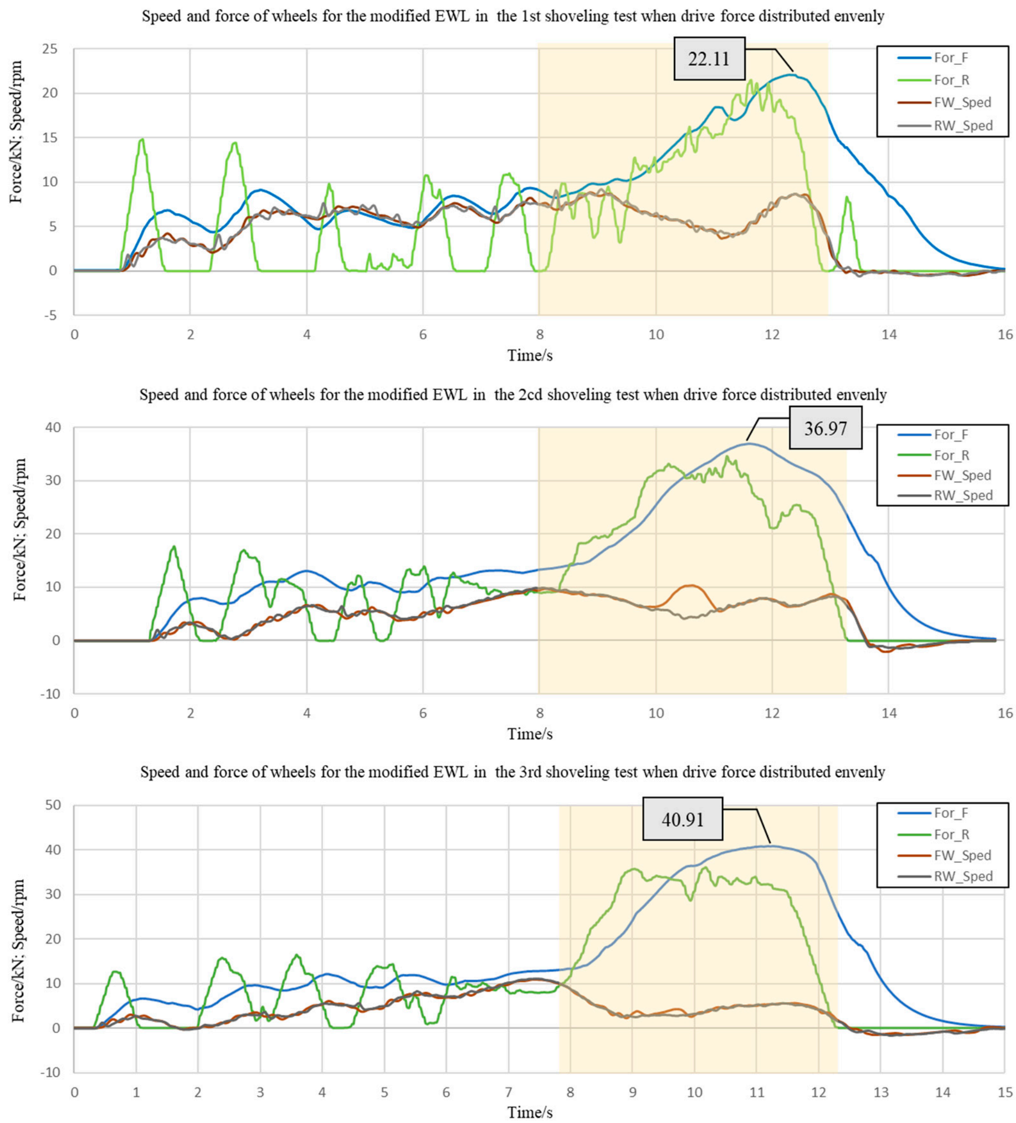

Figure 12. Speed and force of drive wheels in shoveling tests under an evenly distributed drive force control method.

In the tests with torque distributed according to wheel load, the maximum torque of the front motor reached 442 Nm, 605 Nm, and 737 Nm, respectively, while the corresponding maximum torque of the rear motor was 479 Nm, 712 Nm, and 995 Nm. The maximum torques on the front and rear wheels were 18,505 Nm and 10,398 Nm in the first test, 25,326 Nm and 15,456 Nm in the second test, and 30,871 Nm and 21,599 Nm in the third test. As shown in Figure 13, when the front wheels reached maximum torque, the rear wheels generated significantly lower torque values, indicating that the rear wheels were under less load. The dashed line in the yellow-marked area indicates the value of the rear wheel force at the moment when the front wheel force reaches its maximum. Notably, during the first and second tests, when the front wheels reached maximum torque, the rear wheels completely slid, but the rear torque dropped to zero, meaning that the rear motor did not output power even though it was still rotating. This suggests that using the drive torque distribution by wheel load control method can reduce energy consumption.

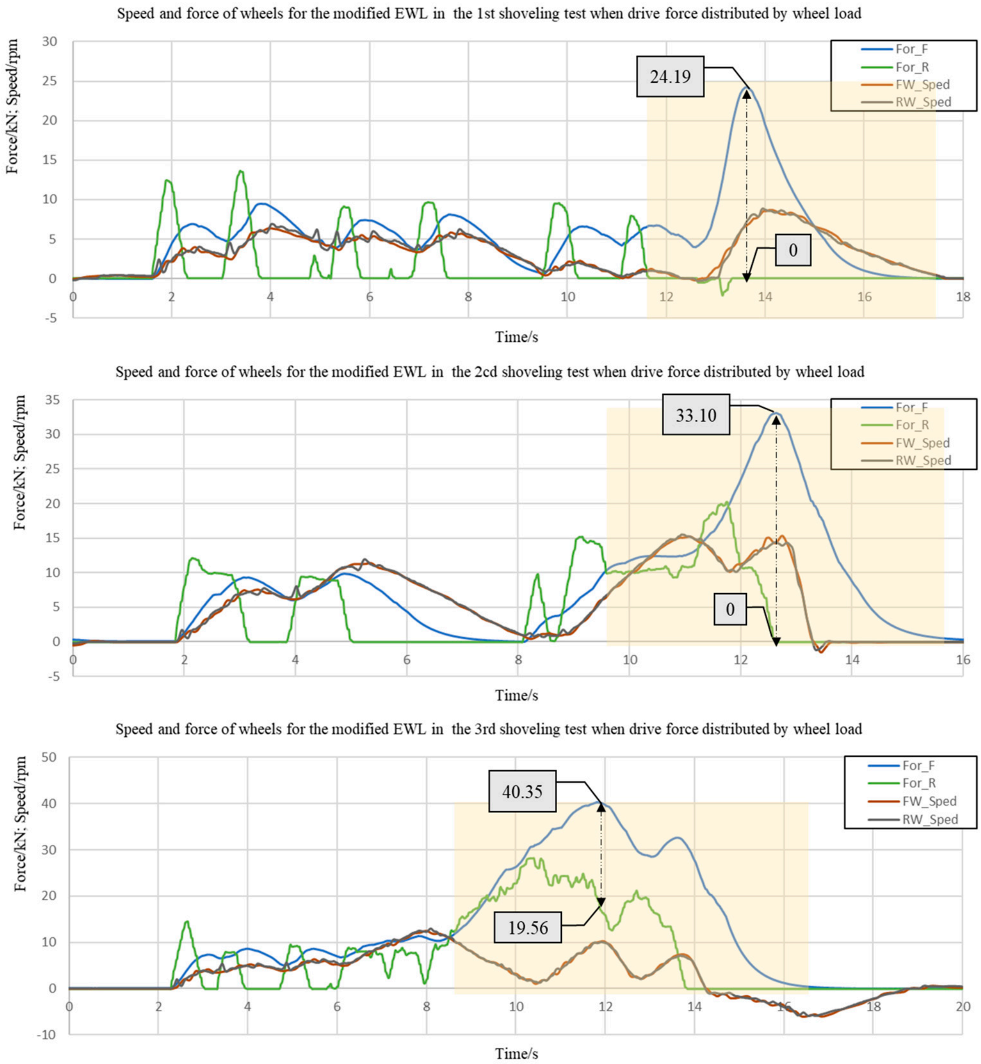

Figure 13. Speed and force of drive wheels in shoveling tests under the drive force distributed by wheel load control method.

5.3. Further Study

Although energy-saving control in loaders is closely related to advancements in drive motor selection and control [23,34], battery management technologies [7,35], hybrid technologies [10,36], and hydraulic system performance [37,38], it is crucial to recognize the substantial influence that operator habits exert on energy consumption. Therefore, research in driver assistance technologies must be intensified, aiming not only to reduce operator workload but also to significantly enhance the efficiency and energy utilization of WLs. This research direction is easier to develop in EWLs, and should encompass the integrated use of dynamic assessment, fuzzy control, image recognition, and machine learning techniques.

6. Conclusions and Limitations

In this case study, the PMSM proves to be more effective in R-drive modes for the EWL, regardless of whether the front wheels are powered by PMSMs or SRMs, or whether the transmission ratio of the front drivetrain is increased. Under walking conditions, power consumption in R-drive mode is 68.56%, 71.88%, and 74.87% of that in F-drive mode at motor speeds of 200 rpm, 400 rpm, and 600 rpm, respectively, as tested on the original EWL. On the modified EWL, with the front transmission ratio nearly doubled, R-drive mode consumes 73.90%, 70.35%, and 67.72% of the power used in F-drive mode at the same motor speeds. This indicates that using the rear motor for single driving under walking conditions can result in significant energy savings.

In shoveling conditions, distributing motor torque according to tire load can enhance driving performance, as this reduces rear wheel slippage and minimizes parasitic power loss. An SRM generates sufficient drive force by multiplying the transmission ratio in the front drivetrain, even if the rear wheels are lifted off the ground during shoveling. This indicates that the manufacturing cost of the EWL can be reduced by increasing the transmission ratio of the front drivetrain, while distributing torque based on wheel load.

For the SRM, the high-efficiency speed range is between 1000 rpm and 1800 rpm under full-load operation, achieving an efficiency of 87.3% to 89.34% in testing. With a a drivetrain transmission ratio of 22.85, the EWL would need to operate at a velocity of 6.64 km/h to 11.95 km/h to maintain high efficiency, assuming a tire diameter of 0.805 m. However, if the transmission ratio is increased to 44.05, the corresponding velocity range decreases to 3.44 km/h to 6.2 km/h, which aligns more closely with the typical operating speeds of a WL, particularly during shoveling operations where the speed is generally very low. Therefore, the SRM on the front drive axle is better suited for shoveling conditions with a larger transmission ratio.

Due to the high experimental costs and the long manufacturing and assembly cycles, this study did not conduct tests and comparisons on EWLs with a wider range of transmission ratios. Additionally, motors other than PMSMs and SRMs were not used as drive motors for testing on EWLs. Future research could incorporate both simulation and real vehicle tests for comparative studies to address the limitations of this case study.

Author Contributions: Methodology, X.F., Y.H. and M.A.A.; software, X.F., Y.H. and P.L.; formal analysis, X.F.; writing—original draft, X.F. and M.A.A.; writing—review and editing, S.V.W.; visualization, P.L.; supervision, Y.H. and S.V.W.; project administration, Y.H. and S.V.W.; funding acquisition, X.F. and P.L. All authors have read and agreed to the published version of the manuscript.

Funding: This research was funded by the Sudian Yingcai Engineering Project from the Jiangsu Vocational College of Electronics and Information, the Huai'an City Science and Technology project grant number (HABZ202319), the Jiangsu Province Vocational College Teachers' Study Visit and Training Program 2024 grant number (2024GRFX066), and Huai'an New Energy Vehicle Technology Public Service Platform grant number (HAP202313). The APC was funded by (HABZ202319) and (HAP202313).

Data Availability Statement: The original data presented in the study are included in the article, further inquiries can be directed to the corresponding author.

Acknowledgments: We extend our heartfelt appreciation to the Jiangsu Province Vocational College Teachers' Study Visit and Training Program 2024 (Program code: 2024GRFX066) as well as the Jiangsu Intelligent Unmanned Equipment Industry Innovation Center for their generous support in providing facilities and accommodation.

Conflicts of Interest: The authors declare no conflicts of interest.

Abbreviations

BLDC	Brushless Direct Current Motor
EV	Electric Vehicle
EWL	Electric Wheel Loader
DEWL	Distributed Electric Drive Wheel Loader
HEV	Hybrid Electric Vehicle
IM	Induction Motor
PMSM	Permanent Magnet Synchronous Motor
SRM	Switched Reluctance Motor
WL	Wheel Loader

Appendix A

Table A1. Test data of peak torque for the SRM (the input voltage is 617 V).

Speed (rpm)	Torque (Nm)	Input Current (V)	Input Power (kW)	Output Power (kW)	Efficiency (%)
205	3230.1	230.5	142.22	69.34	48.75
302	3068.8	253.4	156.35	97.04	62.06
403	2927.2	278.6	171.90	123.52	71.86
502	2690.4	300.3	185.29	141.42	76.32
602	2414	305.8	188.68	152.17	80.65

The performance of the SRM and controller system at speeds of 600 rpm and below shows that at 200 rpm, the motor's maximum output torque reaches 3230.1 Nm. At speeds of 500 rpm and below, the output torque consistently exceeds 2500 Nm. When the output torque reaches 3230.1 Nm at 200 rpm, the peak phase current reaches 600 A.

Table A2. Test data of rated speed for the SRM (the input voltage is 619 V).

Speed (rpm)	Torque (Nm)	Input Current (V)	Input Power (kW)	Output Power (kW)	Efficiency (%)
1001	959.5	176.9	109.50	100.57	91.85
1002	1724.6	329.3	203.84	180.95	88.77

The performance of the SRM and controller system at 100 kW output power indicates a system efficiency of 91.85% when the motor operates at its rated power. Given a controller efficiency of approximately 98.5%, the motor efficiency is calculated to be 93.25%. At peak power levels exceeding 180 kW, when the motor delivers 180.95 kW, the system efficiency drops to 88.77%. Assuming the same controller efficiency of 98.5%, the motor efficiency at this peak power is calculated to be 90.12%.

Table A3 presents the data from the full-load performance test of the SRM, which aims to verify the torque, power, and energy efficiency when the accelerator pedal is fully engaged.

Table A3. Test data of rated speed for the SRM (the input voltage is 619 V).

Speed (rpm)	Torque (Nm)	Input Current (V)	Input Power (kW)	Output Power (kW)	Efficiency (%)
205	3230.1	230.5	142.22	69.34	48.75
403	2927.2	278.6	171.90	123.52	71.86
602	2414	305.8	188.68	152.17	80.65
802	2001.1	315.5	194.66	168.05	86.33
1002	1724.6	329.3	203.84	180.95	88.77
1201	1365.4	310.5	192.20	171.71	89.34
1401	1127	302.6	187.31	165.33	88.27
1601	915.7	280.4	173.57	153.51	88.44
1801	748.5	261.2	161.68	141.16	87.30
2001	625.2	250.7	155.18	131.00	84.41
2201	538.1	236.3	146.27	124.02	84.79
2401	451.5	220.5	136.49	113.51	83.17
2601	384.7	204.5	126.59	104.78	82.77
2801	339.7	194.1	120.15	99.63	82.93
3002	285.5	180.3	111.61	89.75	80.41

Appendix B

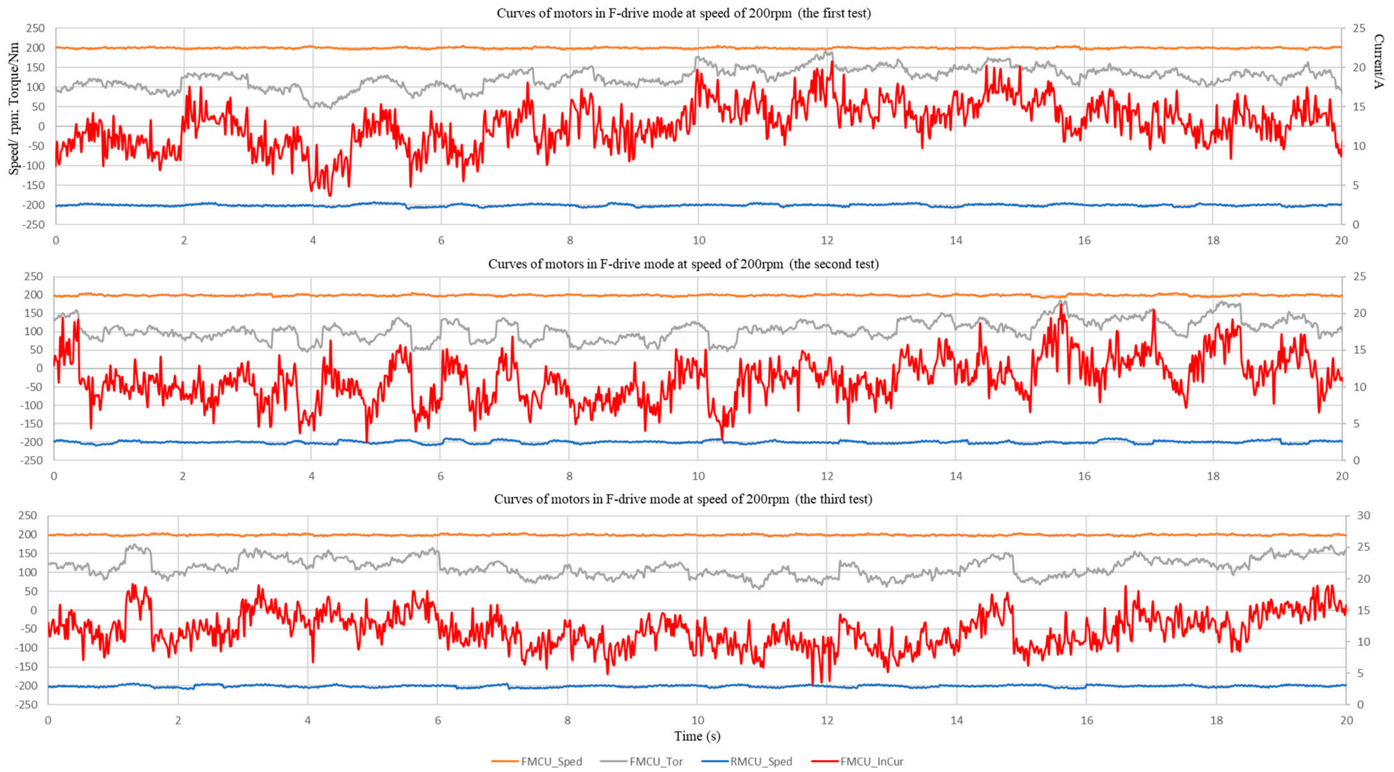

Figure A1. Speed, torque, and current curves of motor when the original EWL is driven by the front PMSM at 200 rpm.

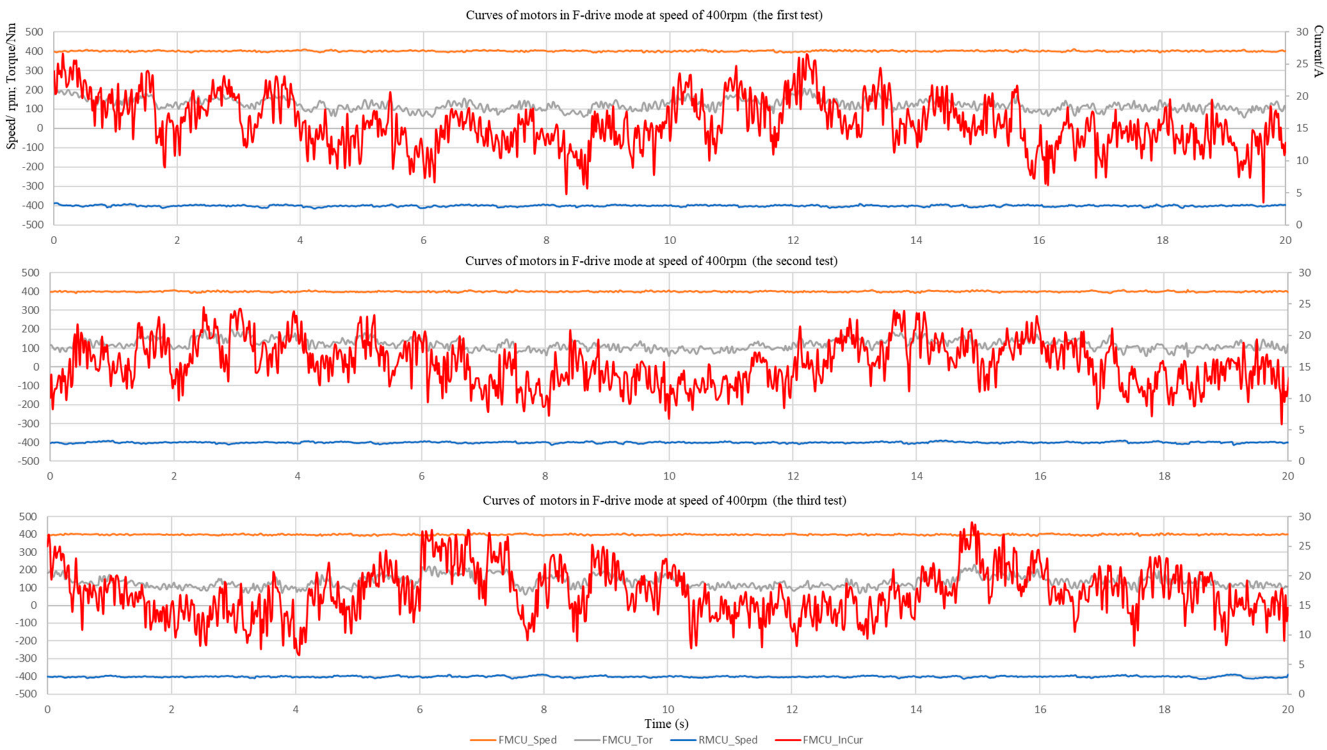

Figure A2. Speed, torque, and current curves of motor when the original EWL is driven by the front PMSM at 400 rpm.

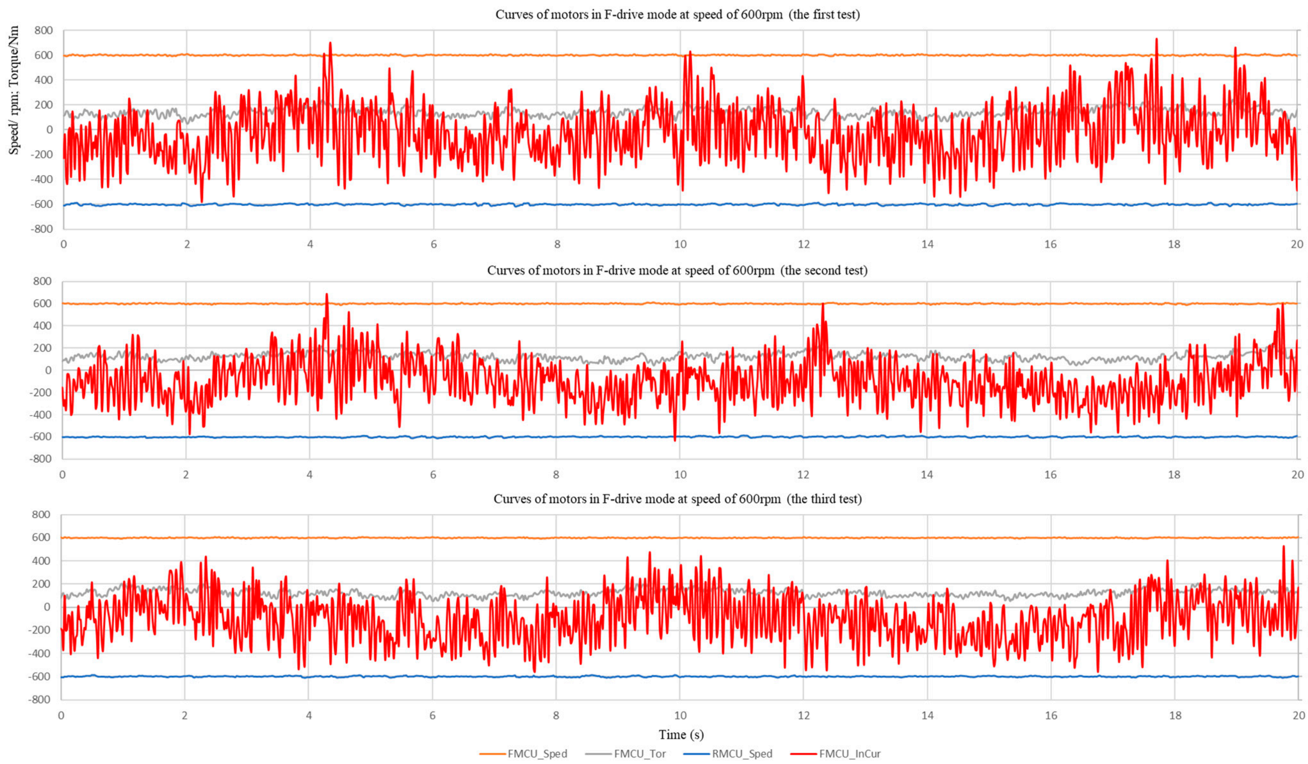

Figure A3. Speed, torque, and current curves of motor when the original EWL is driven by the front PMSM at 600 rpm.

Figure A4. Speed, torque, and current curves of motor when the original EWL is driven by the rear PMSM at 200 rpm.

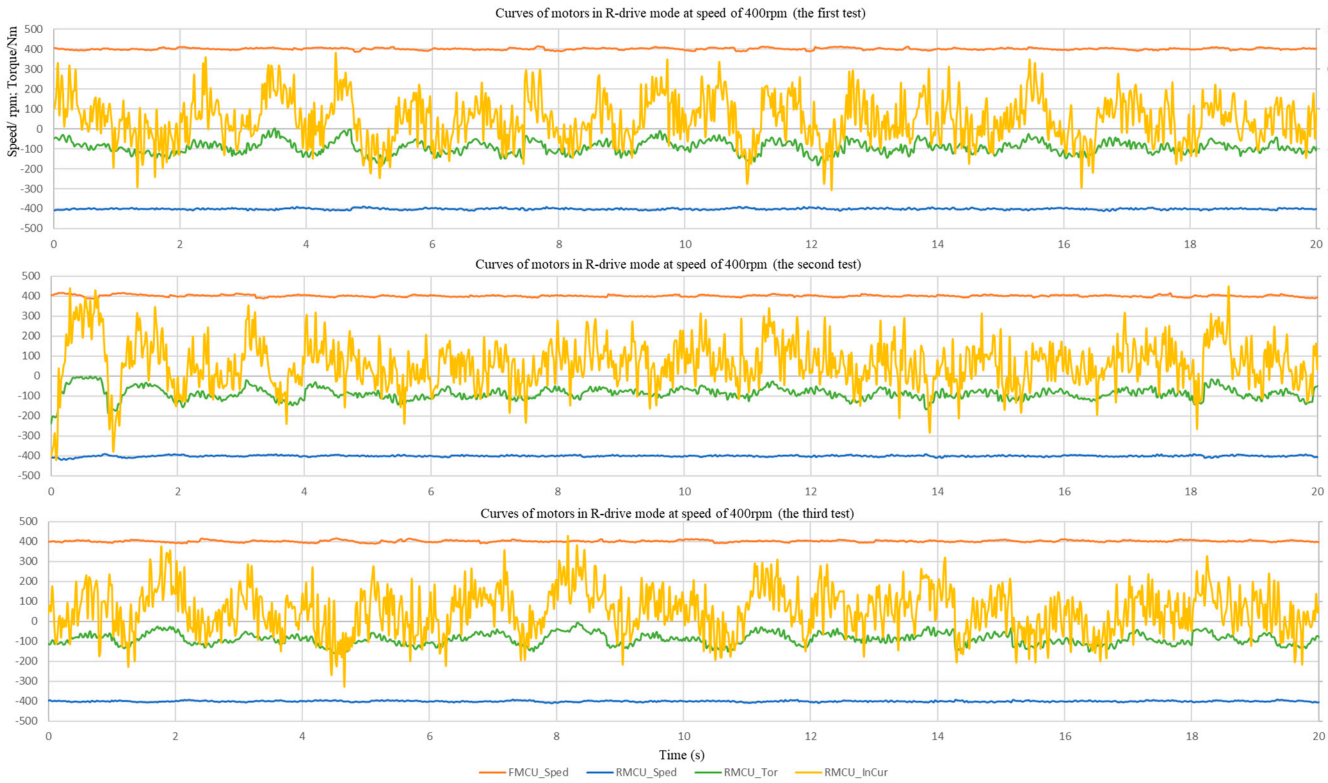

Figure A5. Speed, torque, and current curves of motor when the original EWL is driven by the rear PMSM at 400 rpm.

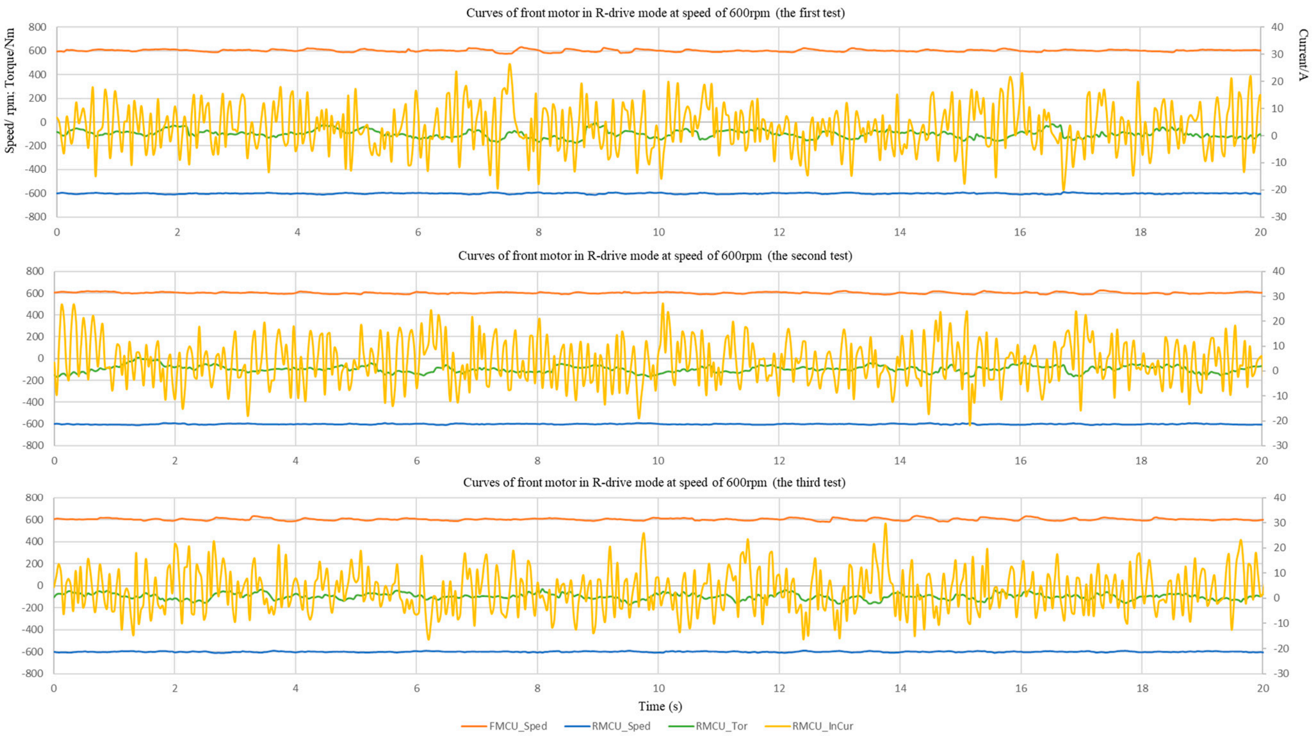

Figure A6. Speed, torque, and current curves of motor when the original EWL is driven by the rear PMSM at 600 rpm.

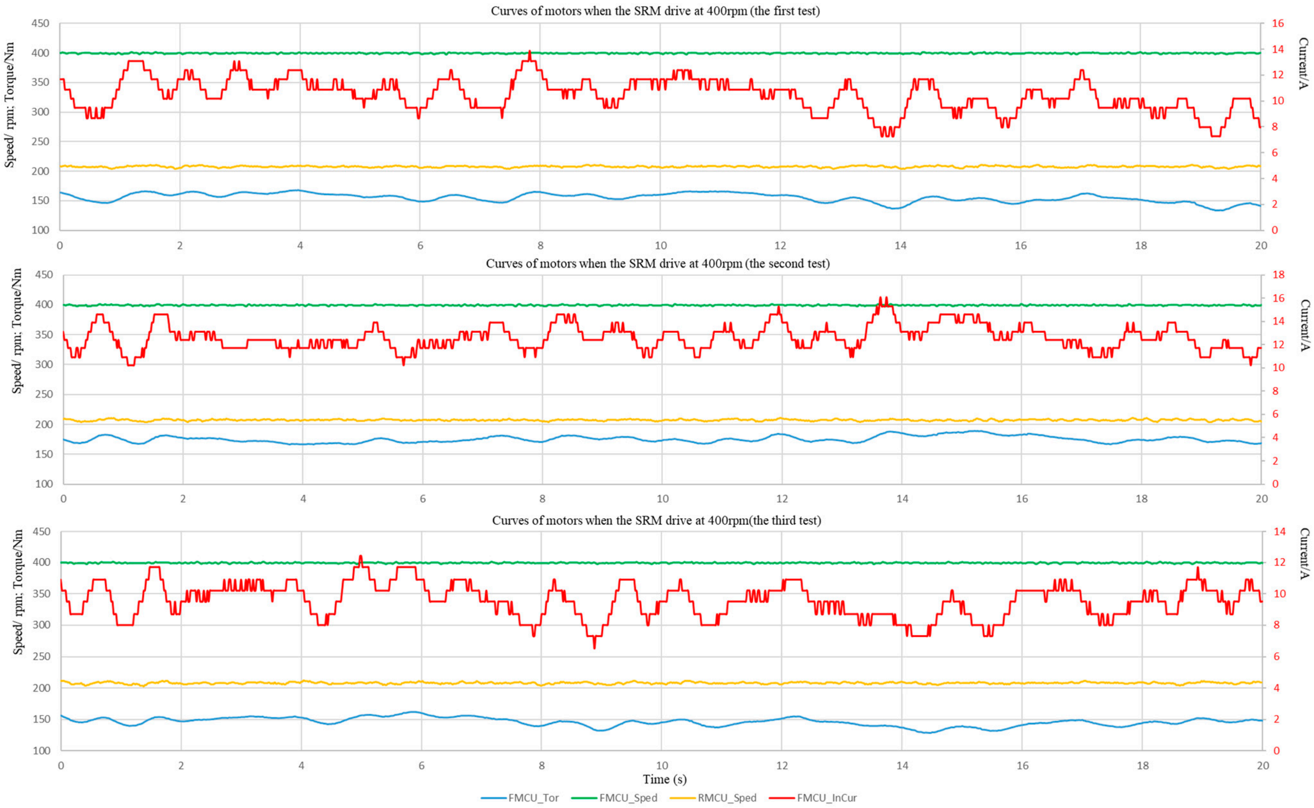

Figure A7. Speed, torque, and current curves of motor when the modified EWL is driven by SRM at 400 rpm.

Figure A8. Speed, torque, and current curves of motor when the modified EWL is driven by SRM at 800 rpm.

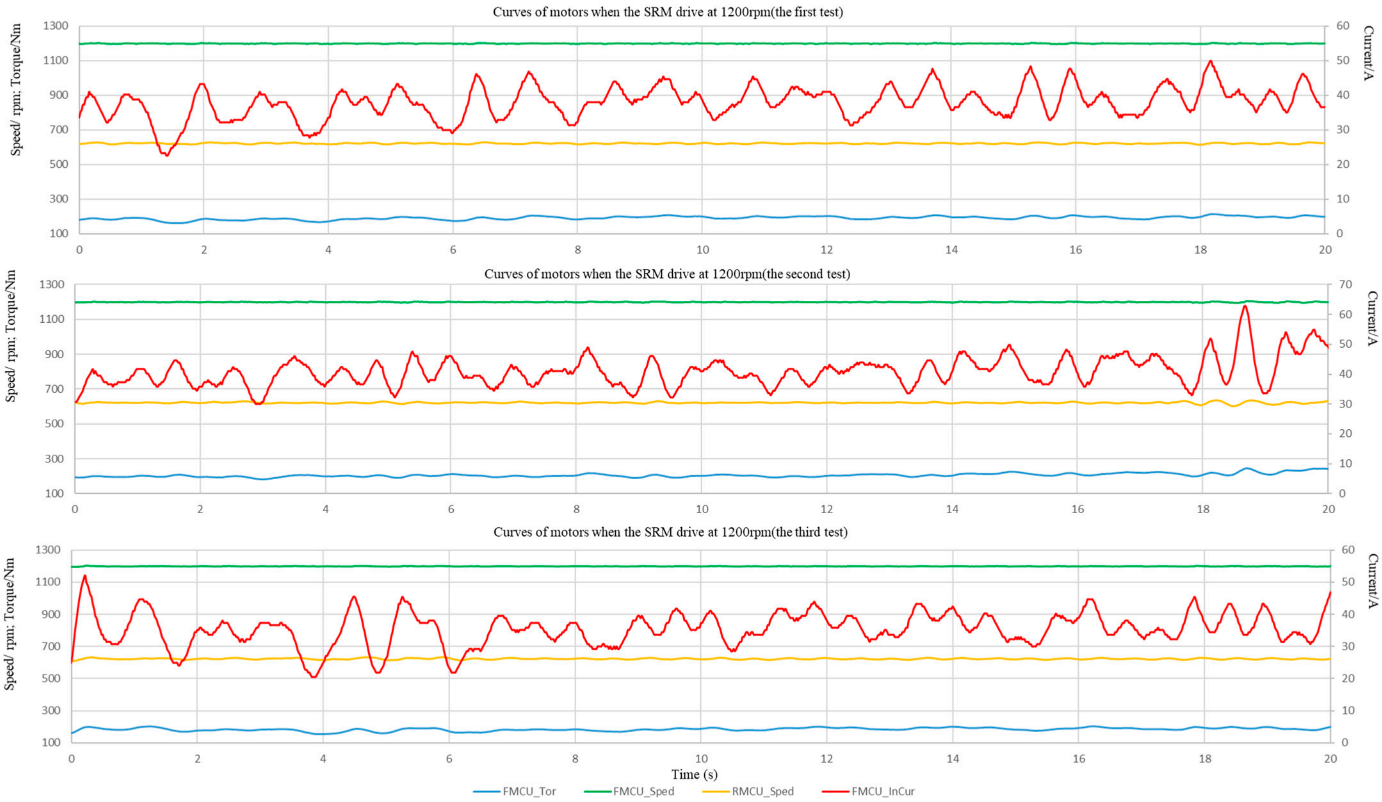

Figure A9. Speed, torque, and current curves of motor when the modified EWL is driven by SRM at 1200 rpm.

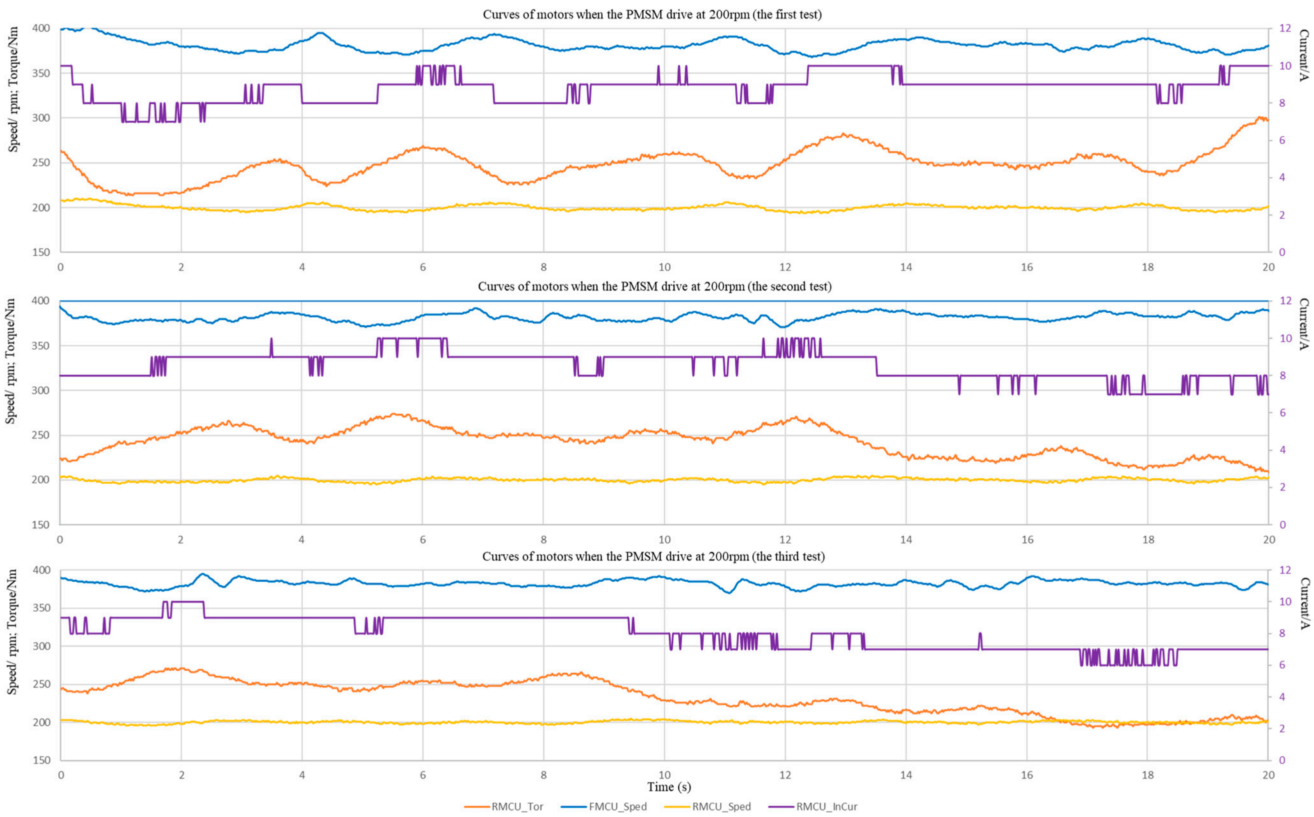

Figure A10. Speed, torque, and current curves of motor when the modified EWL is driven by PMSM at 200 rpm.

Figure A11. Speed, torque, and current curves of motor when the modified EWL is driven by PMSM at 400 rpm.

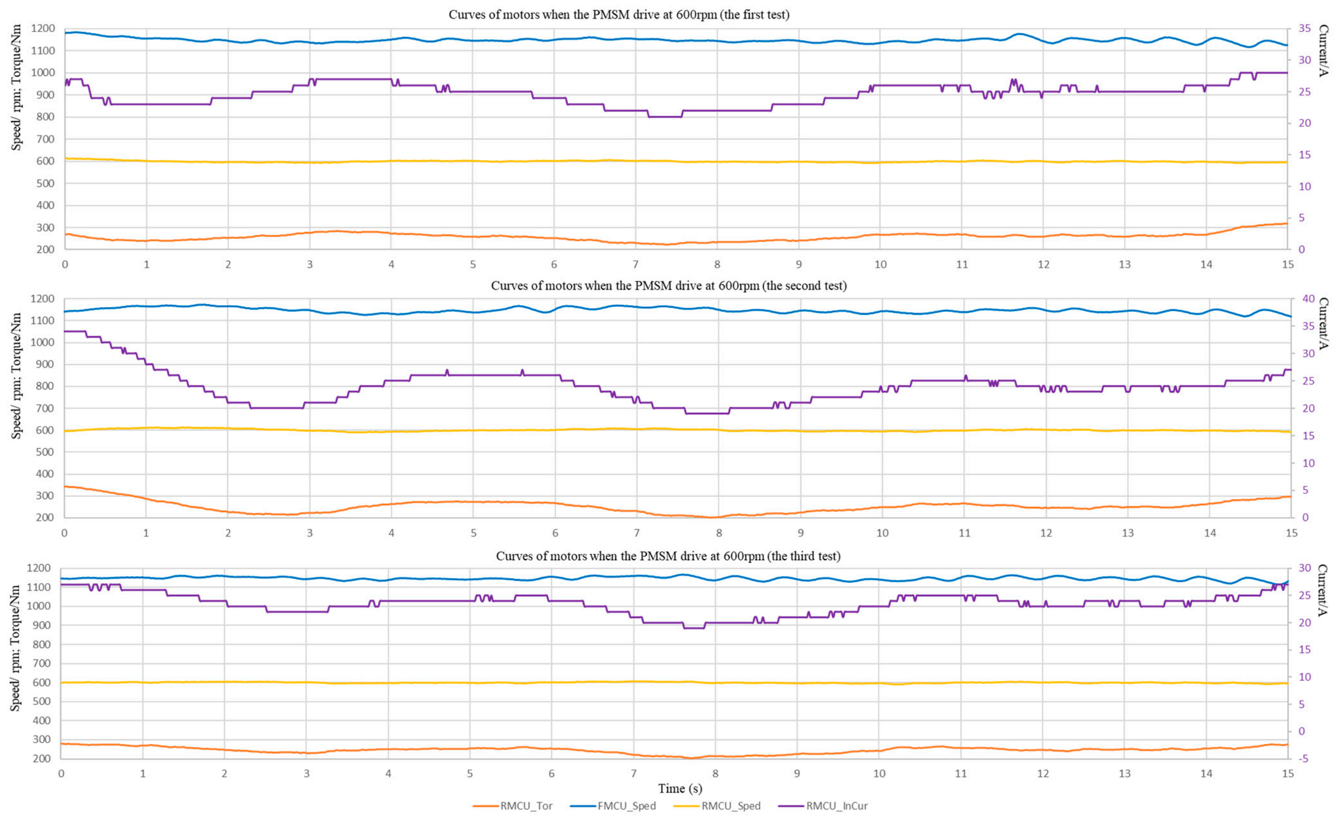

Figure A12. Speed, torque, and current curves of motor when the modified EWL is driven by PMSM at 600 rpm.

References

1. Cunanan, C.; Tran, M.-K.; Lee, Y.; Kwok, S.; Leung, V.; Fowler, M. A review of heavy-duty vehicle powertrain technologies: Diesel engine vehicles, battery electric vehicles, and hydrogen fuel cell electric vehicles. *Clean Technol.* **2021**, *3*, 474–489. [CrossRef]
2. Naumanen, M.; Uusitalo, T.; Huttunen-Saarivirta, E.; van der Have, R. Development strategies for heavy duty electric battery vehicles: Comparison between China, EU, Japan and USA. *Resour. Conserv. Recycl.* **2019**, *151*, 104413. [CrossRef]
3. Mo, Y. Design and Development of Drive System of Pure Electric Loader. *Constr. Mach. Equip.* **2022**, *53*, 11–12+83–86. Available online: https://www.cnki.net/kns/defaultresult/index (accessed on 20 August 2024).
4. Lin, T.; Lin, Y.; Ren, H.; Chen, H.; Chen, Q.; Li, Z. Development and key technologies of pure electric construction machinery. *Renew. Sustain. Energy Rev.* **2020**, *132*, 110080. [CrossRef]
5. Li, Z.; Lin, T.; Gao, Q. Energy consumption prediction of electric construction machinery based on condition identification. *IEEE Access* **2022**, *10*, 127461–127468. [CrossRef]
6. Oh, K.; Kim, H.; Ko, K.; Kim, P.; Yi, K. Integrated wheel loader simulation model for improving performance and energy flow. *Autom. Constr.* **2015**, *58*, 129–143. [CrossRef]
7. Zhang, H.; Wang, F.; Xu, B.; Fiebig, W. Extending battery lifetime for electric wheel loaders with electric-hydraulic hybrid powertrain. *Energy* **2022**, *261*, 125190. [CrossRef]
8. Shafikhani, I. Energy management of hybrid electric vehicles with battery aging considerations: Wheel loader case study. *Control Eng. Pract.* **2021**, *110*, 104759. [CrossRef]
9. Gao, R.; Zhou, G.; Wang, Q. Real-time three-level energy management strategy for series hybrid wheel loaders based on WG-MPC. *Energy* **2024**, *295*, 131011. [CrossRef]
10. Lin, Z.; Lin, Z.; Wang, F.; Xu, B. A series electric hybrid wheel loader powertrain with independent electric load-sensing system. *Energy* **2024**, *286*, 129497. [CrossRef]
11. Wang, F.; Zhang, Q.; Wen, Q.; Xu, B. Improving productivity of a battery powered electric wheel loader with electric-hydraulic hybrid drive solution. *J. Clean. Prod.* **2024**, *440*, 140776. [CrossRef]
12. Wang, F.; Lin, Z.; Xu, B.; Fiebig, W. An electric-hydrostatic energy storage system for hydraulic hybrid wheel loader. *IEEE Trans. Veh. Technol.* **2022**, *71*, 7044–7056. [CrossRef]
13. Zhang, H.; Wang, F.; Lin, Z.; Xu, B. Optimization of speed trajectory for electric wheel loaders: Battery lifetime extension. *Appl. Energy* **2023**, *351*, 121865. [CrossRef]
14. Mu, H.; Luo, Y.; Luo, Y.; Chen, L. Simulation Study on Variable Pressure Margin Energy Recovery of Electric Loader Actuator. *Electronics* **2022**, *11*, 4215. [CrossRef]
15. Yang, Y.; He, Q.; Fu, C.; Liao, S.; Tan, P. Efficiency improvement of permanent magnet synchronous motor for electric vehicles. *Energy* **2020**, *213*, 118859. [CrossRef]
16. Minh, D.B.; Quoc, V.D.; Huy, P.N. Efficiency Improvement of Permanent Magnet BLDC Motors for Electric Vehicles. *Eng. Technol. Appl. Sci. Res.* **2021**, *11*, 7615–7618. [CrossRef]
17. Dorrell, D.G.; Knight, A.M.; Popescu, M.; Evans, L.; Staton, D.A. Comparison of different motor design drives for hybrid electric vehicles. In Proceedings of the 2010 IEEE Energy Conversion Congress and Exposition, Atlanta, GA, USA, 12–16 September 2010; pp. 3352–3359.
18. Wu, J.; Liang, J.; Ruan, J.; Zhang, N.; Walker, P.D. Efficiency comparison of electric vehicles powertrains with dual motor and single motor input. *Mech. Mach. Theory* **2018**, *128*, 569–585. [CrossRef]
19. Xiaolin, J.; Laide, S.; Yongming, B. Design and research on wheel-driven systems of electric loaders. *Chin. J. Constr. Mach.* **2010**, *8*, 62–65+71. [CrossRef]
20. Li, T.; Liu, H.; Zhao, D.; Wang, L. Design and analysis of a fuel cell supercapacitor hybrid construction vehicle. *Int. J. Hydrogen Energy* **2016**, *41*, 12307–12319. [CrossRef]
21. Liu, G.; Liu, L.; Chen, S.-X. The study of switched reluctance motor drive system for heavy vehicles. In Proceedings of the 2014 IEEE Conference and Expo Transportation Electrification Asia-Pacific (ITEC Asia-Pacific), Beijing, China, 31 August–3 September 2014; pp. 1–5.
22. Yildirim, M.; Polat, M.; Kürüm, H. A survey on comparison of electric motor types and drives used for electric vehicles. In Proceedings of the 2014 16th International Power Electronics and Motion Control Conference and Exposition, Antalya, Turkey, 21–24 September 2014; pp. 218–223.
23. Li, X.; Duan, C.; Bai, K.; Yao, Z. Operating Performance of Pure Electric Loaders with Different Types of Motors Based on Simulation Analysis. *Energies* **2021**, *14*, 617. [CrossRef]
24. Fei, X.; Han, Y.; Wong, S.V.; Azman, M.A. Efficiency Comparison of Electric Wheel Loader Powertrains with Dual Motor Input in Distributed Driving Modes. *World Electr. Veh. J.* **2023**, *14*, 298. [CrossRef]
25. Mitschke, M.; Wallentowitz, H. *Dynamik der Kraftfahrzeuge*; Springer: Berlin/Heidelberg, Germany, 1972.
26. Cao, B.; Liu, X.; Chen, W.; Li, H.; Wang, X. Intelligentization of wheel loader shoveling system based on multi-source data acquisition. *Autom. Constr.* **2023**, *147*, 104733. [CrossRef]
27. Wang, S.; Yin, Y.; Wu, Y.; Hou, L. Modeling and Verification of an Acquisition Strategy for Wheel Loader's Working Trajectories and Resistance. *Sensors* **2022**, *22*, 5993. [CrossRef]
28. Madau, R.; Colombara, D.; Alexander, A.; Vacca, A.; Mazza, L. An online estimation algorithm to predict external forces acting on a front-end loader. *Proc. Inst. Mech. Eng. Part I J. Syst. Control. Eng.* **2021**, *235*, 1678–1697. [CrossRef]

29. Chen, Y.; Shi, G.; Jiang, H.; Zheng, T. Research on the prediction of insertion resistance of wheel loader based on pso-lstm. *Appl. Sci.* **2023**, *13*, 1372. [CrossRef]
30. Yang, Z.; Wang, Z.; Zhang, C. *Wheel Loader*; Chemical Industry Press: Beijing, China, 2005.
31. Gao, G.; Wang, J.; Ma, T.; Han, Y.; Yang, X.; Li, X. Optimisation strategy of torque distribution for the distributed drive electric wheel loader based on the estimated shovelling load. *Veh. Syst. Dyn.* **2022**, *60*, 2036–2054. [CrossRef]
32. Guo, H.; Sun, Q.; Wang, C.; Wang, Q.; Lu, S. A systematic design and optimization method of transmission system and power management for a plug-in hybrid electric vehicle. *Energy* **2018**, *148*, 1006–1017. [CrossRef]
33. Fei, X.; Shenrui, H.; Voon, W.S.; Azman, M.A.; Yunwu, H. Mechanical Characteristics of Distributed Electric Wheel Loader in Shoveling Condition. *Automot. Exp.* **2023**, *6*, 336–358. [CrossRef]
34. Haoling, R.; Shaole, C.; Qihuai, C.; Tianliang, L.; Bin, L. Shift Strategy of Electric Drive Loader with Compound Control of Motor and Clutch. *J. Shanghai Jiaotong Univ.* **2022**, *56*, 173.
35. Huang, X.; Huang, Q.; Cao, H.; Wang, Q.; Yan, W.; Cao, L. Battery capacity selection for electric construction machinery considering variable operating conditions and multiple interest claims. *Energy* **2023**, *275*, 127454. [CrossRef]
36. Zeng, X.; Yang, N.; Peng, Y.; Zhang, Y.; Wang, J. Research on energy saving control strategy of parallel hybrid loader. *Autom. Constr.* **2014**, *38*, 100–108. [CrossRef]
37. Zhang, W.; Zhou, J.; Zhang, Y.; Huang, P.; Deng, J. Energy—Saving analysis in the hydraulic system of loader working device. *Int. J. Comput. Appl. Technol.* **2012**, *45*, 106–114. [CrossRef]
38. Wang, F.; Wen, Q.; Xu, B. An energy saving rule-based strategy for electric-hydraulic hybrid wheel loaders. *Proc. Inst. Mech. Eng. Part D J. Automob. Eng.* **2023**, *230*, 09544070231191843. [CrossRef]